

國立臺灣大學理學院數學研究所

碩士論文

Department of Mathematics

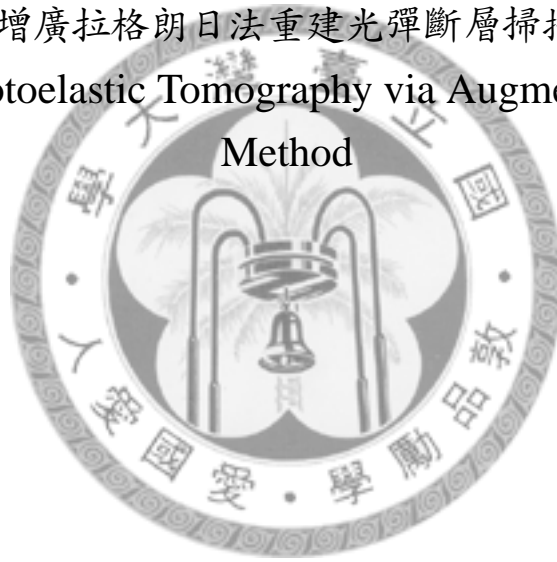
College of Science

National Taiwan University

Master Thesis

利用增廣拉格朗日法重建光彈斷層掃描影像

Reconstruct Photoelastic Tomography via Augmented Lagrangian
Method



吳浩平

Hao-Pin Wu

指導教授：陳宜良 教授

Advisor: I-Liang Chern, Professor

中華民國 100 年 7 月

July, 2011

中文摘要

集成光彈是一藉由偏振光學技術來測定光彈材料內應力分佈的方法，其造影模型可由 Sharafutdinov 提出的截斷橫向射線變換所描述。在這篇論文中，我們利用此一模型將其重建問題置於 TV-L2 極小化的框架下，並結合代數重建法和增廣拉格朗日法提出其對應的數值重建過程。

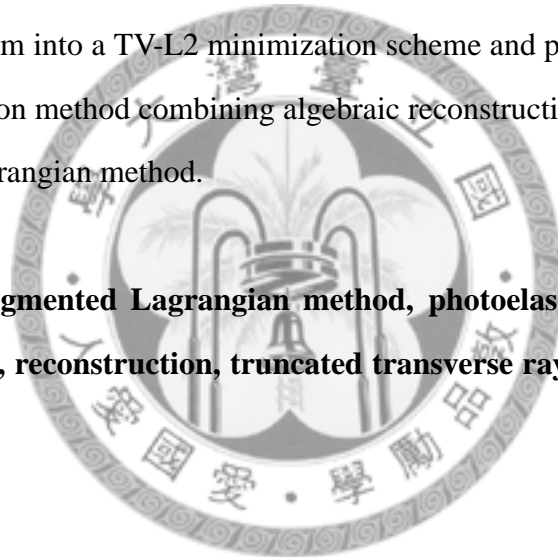
關鍵字：增廣拉格朗日法、光彈斷層掃描、偏振光、重建、截斷橫向射線變換、總變差正規化



Abstract

Integrated photoelasticity is a method for determining stress distribution in photoelastic materials by polarized optical techniques. An important model describes the imaging process is truncated transverse ray transform (TTRT) proposed by Sharafutdinov. In this article, we use this model to fit the reconstruction problem into a TV-L2 minimization scheme and propose a numerical reconstruction method combining algebraic reconstruction technique and augmented Lagrangian method.

Keywords: augmented Lagrangian method, photoelastic tomography, polarized light, reconstruction, truncated transverse ray transform, TV regularization



Contents

中文摘要	i
Abstract	ii
1 Introduction	1
2 Photoelasticity	3
2.1 Stress-Optic Law	3
2.2 Polarization of Light waves	7
2.3 Integrated Photoelasticity	11
2.4 Transverse Ray Transform	14
2.5 The Polarization Ellipse	16
2.6 Truncated Transverse Ray Transform	19
3 Reconstruction Methods	21
3.1 Aben's method	21
3.2 Sharafutdinov's Methods	24
3.3 Lioheart and Sharafutdinov's Method	25
3.3.1 Logitudinal Ray Transform (LRT)	26
3.3.2 Inversion Formula of LRT	27
3.3.3 Algebraic Equations in Fourier Space	28
4 Augmented Lagrangian Method	30
4.1 Augmented Lagrangian Method	30
4.2 Alternating Direction Method	31
5 Numerical Results	33
5.1 Numerical Settings	33
5.2 Results	33
5.3 Summary	47
6 Conclusion and Future Works	48
Bibliography	50

List of Figures

2.1	Birefringence	5
2.2	Two kinds of tensor fields	6
2.3	Different types of polarizations (section by a plane)	9
2.4	Different types of polarization	9
2.5	Illustration of the change of polarization	10
2.6	Polarization Ellipse	18
3.1	Aben's Method	23
5.1	Testing Tensor Phantom	35
5.2	Reconstruction by gradient descent method with 3 η 's.	36
5.3	Reconstruction by gradient descent method with 6 η 's.	37
5.4	Reconstruction by gradient descent method with 9 η 's.	38
5.5	Reconstruction by ADM with 3 η 's.	39
5.6	Reconstruction by ADM with 6 η 's.	40
5.7	Reconstruction by ADM with 9 η 's.	41
5.8	Comparison among different number of η 's for gradient descent method.	42
5.9	Comparison among different number of η 's for ADM.	43
5.10	Comparison between gradient descent method for 3 η 's.	44
5.11	Comparison between gradient descent method for 6 η 's.	45
5.12	Comparison between gradient descent method for 9 η 's.	46

Chapter 1

Introduction

In some situations, a ray of light split into two when passing through certain anisotropic materials. This phenomenon is called *birefringence* or *double refraction*. Materials possess this property can be found naturally, especially in crystals. Besides, many non-crystalline transparent materials, e.g. glass, which are ordinarily optically isotropic, also display such property under stress. This phenomenon is known as *artificial double refraction* now and was first observed by Scottish physicist David Brewster in 1816. Such materials are called *photoelastic materials*.

The reason why stress changes the optical property of photoelastic materials is because it induces a perturbation on dielectric permittivity. The relation between them is described by the following formula given by Maxwell in 1852:

$$\varepsilon = \varepsilon_0 \delta + C_0 (\sigma - \frac{1}{3} \text{tr}(\sigma) \delta) + C_1 \text{tr}(\sigma) \delta. \quad (1.0.1)$$

Here, ε is the dielectric permittivity tensor; σ is the stress tensor; δ is the Kronecker 3-by-3 identity tensor; C_0 and C_1 are positive constants.

Photoelasticity is a method for determining the dielectric permittivity (thereby the stress distribution) of a photoelastic material via polarized optical techniques. The *integrated photoelasticity*, proposed in [1], measures the changes of polarization of EM waves passing through the object at various positions and angles. These changes can be characterized by so-called *truncated transverse ray transform* (TTRT)[6], from which, the trace-free part of the dielectric permittivity tensor is constructed. Although the transverse ray transform is similar to the ray transform in X-ray CT, it involves reconstruction of tensor fields instead of scalar fields and remains much less explored.

In this paper, we adopt the forementioned TTRT imaging model and formulate the above reconstruction problem as a TV-L2 minimization problem. Both the gradient-descent method and the augmented Lagrangian method are implemented for solving the minimization problems and results are compared. This paper is organized as follows:

In Section 2, we introduce the principle of photoelasticity, and then, following [6], we derive the TTRT model for integrated photoelasticity.

In Section 3, we review some existing reconstruction methods.

In Section 4, we introduce augmented Lagrangian method, and apply it to the reconstruction problem given by integrated photoelasticity. Our numerical method would be also presented in this section.

In Section 5, we will show our numerical results.

Finally, we summarise and give comments.



Chapter 2

Photoelasticity

2.1 Stress-Optic Law

Birefringence, or double refraction, is the phenomenon that a ray is decomposed into two when it passes through certain materials, see Figure 2.1. Naturally, this optical anisotropy can be found in most crystals. Besides crystals, many non-crystalline materials, which are ordinarily optically isotropic, also display such property under stress. This adventitious anisotropy is known for artificial double refraction and was first observed by Sir David Brewster in 1816, and this kind of materials is called photoelastic materials.

In fact, in photoelastic materials, stress influences its optical property by changing its dielectric permittivity. When anisotropy is taken into consideration, both stress and permittivity are modeled by second order symmetric tensors, see Figure 2.2. In 1852, Maxwell proposed a **stress-optic law**, which gave a relation between these two tensor fields:

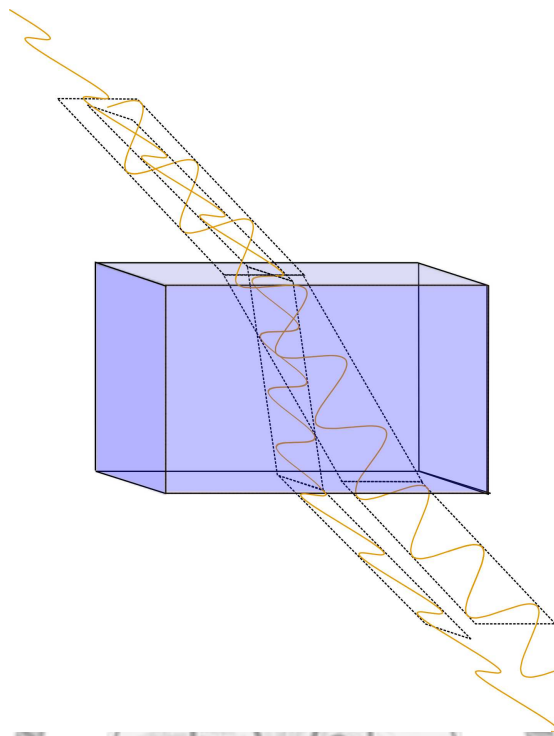
$$\varepsilon = \varepsilon_0 \delta + C_0 (\sigma - \frac{1}{3} \text{tr}(\sigma) \delta) + C_1 \text{tr}(\sigma) \delta. \quad (2.1.1)$$

Here δ is the Kronecker delta, and $\varepsilon_0 \delta$ represents the original isotropic permittivity; σ and ε are stress and the result permittivity, respectively; C_1 and C_2 are positive constants depend only on materials.

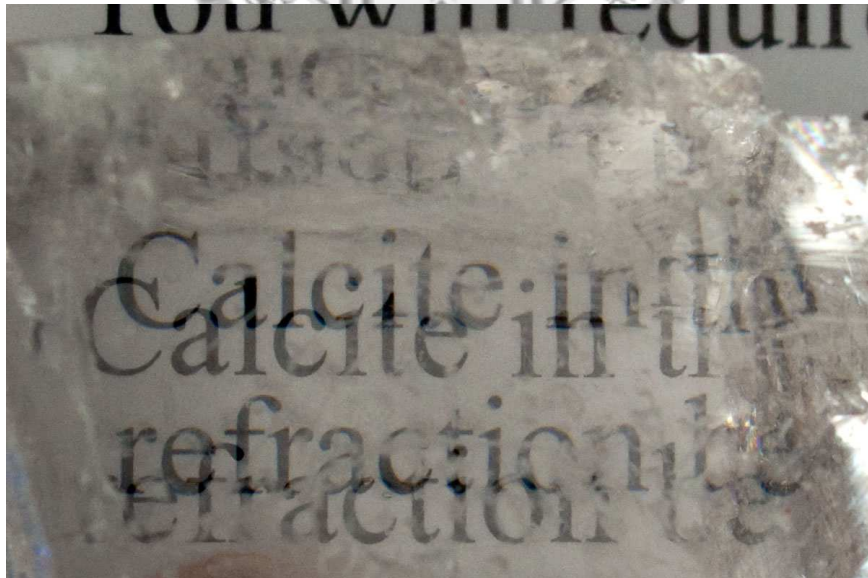
Stress-optic law states that stress induces a perturbation on permittivity in a photoelastic materials, and this “perturbation” is the linear combination of the trace part and the trace-free part of the stress tensor. Photoelasticity is a method which uses polarized optical techniques to reconstruct the permittivity, and thereby the stress distribution of a

photoelastic material.



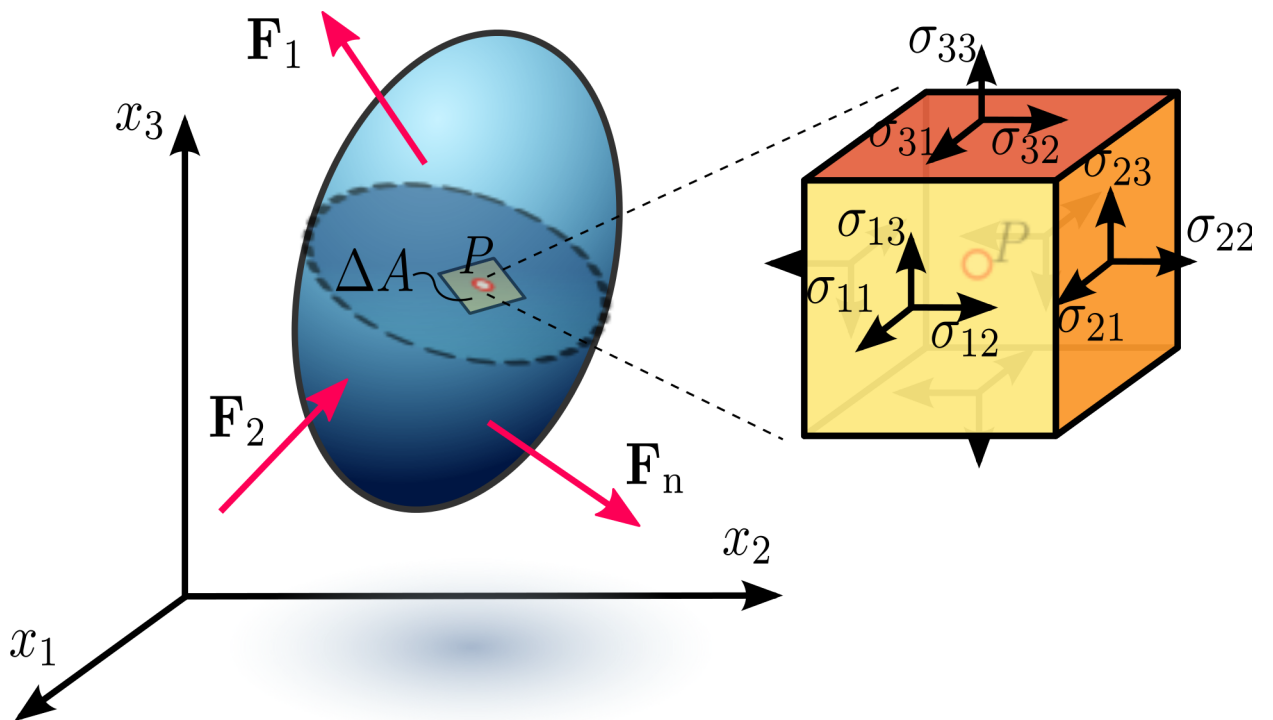


(a) Displacement of light rays with perpendicular polarization through a birefringent material (from Wikipedia)

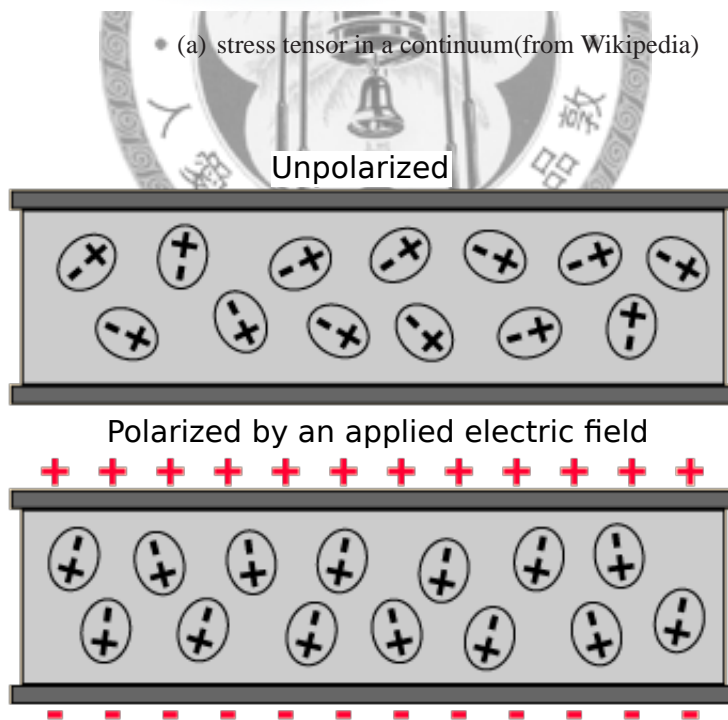


(b) A calcite crystal laid upon a paper with all letters showing the double refraction (from Wikipedia)

Figure 2.1: Birefringence



(a) stress tensor in a continuum(from Wikipedia)



(b) In a dielectric medium, permittivity is the linear transform between the external electric field and the induced polarization.(from Wikipedia)

Figure 2.2: Two kinds of tensor fields

2.2 Polarization of Light waves

In a transverse wave, polarization is the property describing the orientation of its oscillation. For a light wave, it consists of electric field vector \mathcal{E} and magnetic field vector \mathcal{H} ; the former is chosen to define the state of polarization since physical interactions with the wave involve the electric field in most optical media.

The polarization of light waves is specified by the electric field vector $\mathcal{E}(\mathbf{x}, t)$ at position $\mathbf{x} = (x, y, z)$ and time t . The time variation of \mathcal{E} of a monochromatic wave is exactly sinusoidal, that is, it oscillate at a definite frequency. If we assume the light is propagating in the z direction, the electric field vector will lie on the x - y plane, furthermore, the x component and the y component of \mathcal{E} can oscillate independently at a definite frequency. This is completely analogous to the classical motion of a two dimensional harmonic oscillator whose general motion is an ellipse. Correspondingly, if we fix a position \mathbf{x} , in general, the trace of the end of the electric field vector forms an ellipse as t evolves. We will derive this general polarization and show some special cases of it.

In the complex-function representation, the electric field vector of a monochromatic plane wave propagating in the z direction is given by

$$\mathcal{E}(z, t) = \mathbf{A}e^{i(\omega t - kz)}, \quad (2.2.1)$$

where \mathbf{A} is a complex vector which lies in the x - y plane. It is the real part of \mathcal{E} has physical meaning

$$\tilde{\mathcal{E}} = \text{Re } \mathcal{E}, \quad (2.2.2)$$

which is called the *light vector*. Now suppose

$$\mathbf{A} = \hat{x}A_x e^{i\delta_x} + \hat{y}A_y e^{i\delta_y}, \quad (2.2.3)$$

where A_x and A_y are positive numbers, \hat{x} and \hat{y} are unit vectors, then the coordinate form of $\tilde{\mathcal{E}} = (\tilde{\mathcal{E}}_x, \tilde{\mathcal{E}}_y)$ can be written as

$$\begin{cases} \tilde{\mathcal{E}}_x &= A_x \cos(\omega t - kz + \delta_x) \\ \tilde{\mathcal{E}}_y &= A_y \cos(\omega t - kz + \delta_y). \end{cases} \quad (2.2.4)$$

The curve described by the end point of $\tilde{\mathcal{E}}$ as time evolves can be obtained by eliminating $\omega t - kz$ between the equations in (2.2.4), we have

$$\left(\frac{\tilde{\mathcal{E}}_x}{A_x}\right)^2 + \left(\frac{\tilde{\mathcal{E}}_y}{A_y}\right)^2 - 2\frac{\cos\delta}{A_x A_y}\tilde{\mathcal{E}}_x\tilde{\mathcal{E}}_y = \sin^2\delta \quad (2.2.5)$$

where

$$\delta = \delta_y - \delta_x. \quad (2.2.6)$$

All the phase angles are defined in the range $-\pi < \delta \leq \pi$.

When $\delta = 0$ or π , (2.2.5) is a line segment; it is called *linear polarization*. When $\delta = \pm\pi/2$ and $A_x = A_y$, (2.2.5) is a circle; it is called *circular polarization*. In other cases, (2.2.5) is an ellipse; it is called *elliptical polarization*. In general, all these cases can be viewed as elliptical polarization, see Figure 2.3 and 2.4.

By using a rotation, we are able to diagonalize (2.2.5)

$$\left(\frac{\tilde{\mathcal{E}}_{x'}}{a}\right)^2 + \left(\frac{\tilde{\mathcal{E}}_{y'}}{b}\right)^2 = 1 \quad (2.2.7)$$

where x' and y' are new set of axes along the principal axes of the ellipse, a and b are the principal axes of the ellipse. We denote the angle from x to x' by ϕ . This gives a complete description of elliptical polarization: its size is described by $\sqrt{a^2 + b^2}$; its shape is described by b/a ; its orientation is described by angle ϕ ; its sense of revolution of $\tilde{\mathcal{E}}$ is described by the sign of $\sin\delta$: the electric vector will revolve in a clockwise direction if $\sin\delta > 0$ and in counterclockwise direction if $\sin\delta < 0$.

When a polarized ray passes through a transparent specimen, its optical property will reflect on the change of polarization. On this foundation, we can extract informations of permittivity in a photoelastic material by polarized rays, see Figure 2.5. An implementation is called *integrated photoelasticity* and will be introduced in the following section.

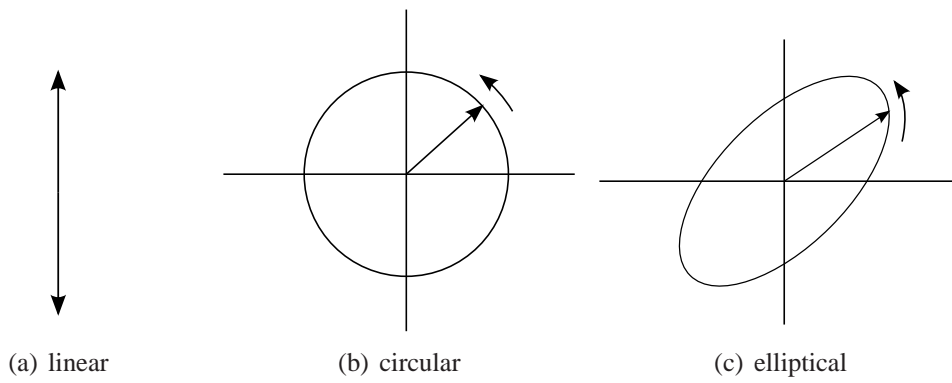


Figure 2.3: Different types of polarizations (section by a plane)

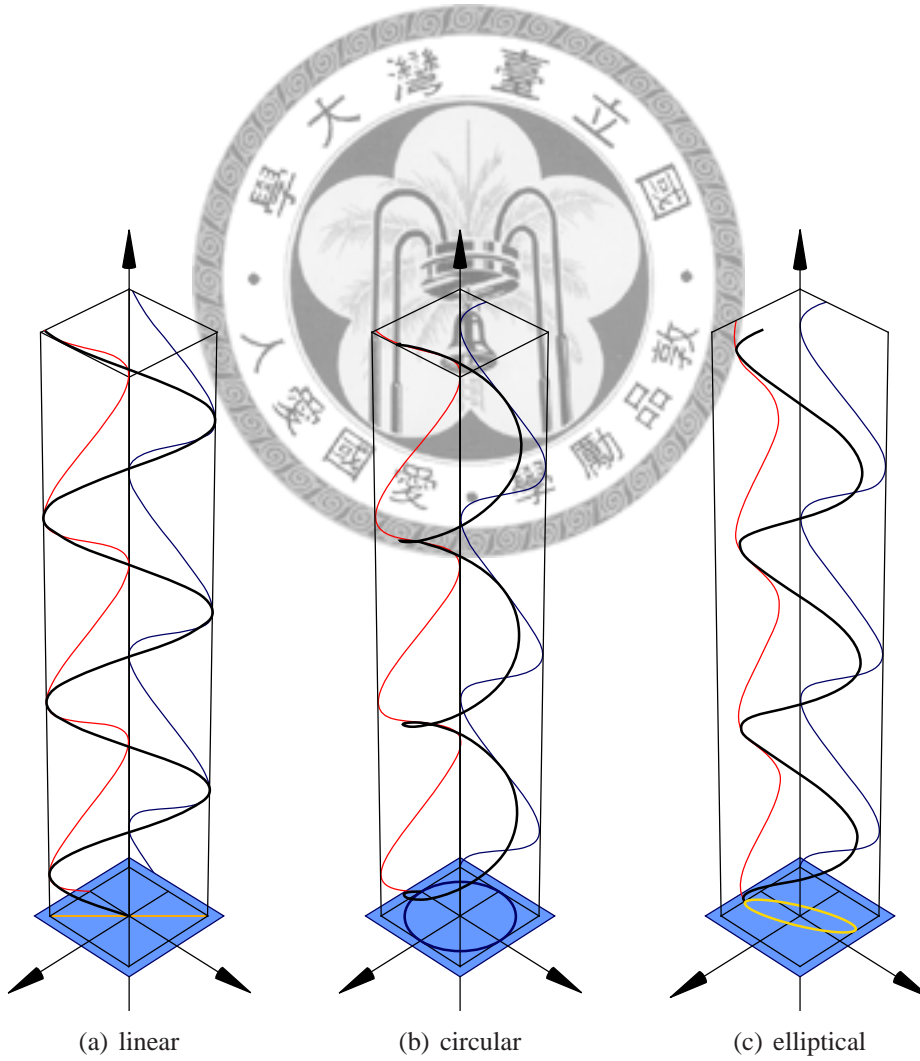


Figure 2.4: Different types of polarization

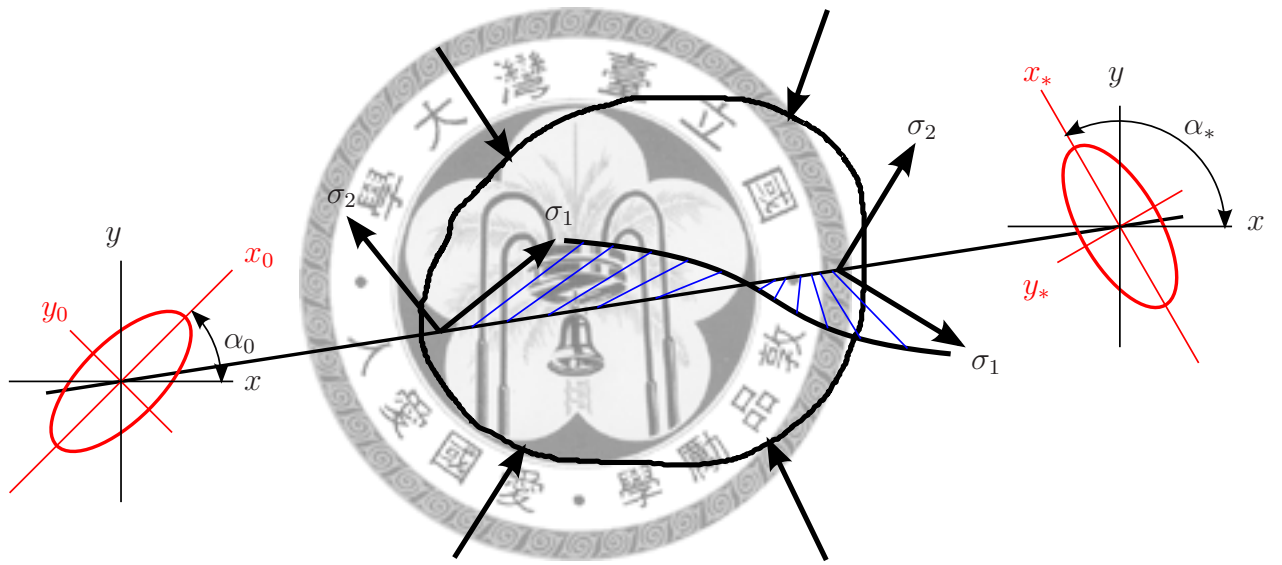


Figure 2.5: Illustration of the change of polarization

2.3 Integrated Photoelasticity

Consider a photoelastic material in three dimensions. We can apply transverse EM wave (light ray) to it to measure the change of its polarization from various angles and positions to extract the information of its permittivity. This method is called *integrated photoelasticity*. Although it is similar to X-ray CT, it involves reconstruction of tensor fields instead of scalar fields and much geometry knowledge is needed.

We begin with the dimensionless Maxwell's equations

$$\begin{cases} \nabla \times \mathcal{H} - \frac{1}{c} \frac{\partial}{\partial t} \mathcal{D} = 0 \\ \nabla \times \mathcal{E} + \frac{1}{c} \frac{\partial}{\partial t} \mathcal{B} = 0 \\ \nabla \cdot \mathcal{D} = 0 \\ \nabla \cdot \mathcal{B} = 0. \end{cases} \quad (2.3.1)$$

In the equations above, \mathcal{H} is the magnetic field, \mathcal{E} is the electric field, \mathcal{D} is the electric displacement field and \mathcal{B} is the magnetic induction. They satisfy the constitutive relation

$$\begin{cases} \mathcal{D} = \varepsilon \mathcal{E}, \\ \mathcal{B} = \mu \mathcal{H}, \end{cases} \quad (2.3.2)$$

where ε is the permittivity tensor and μ is the magnetic permeability tensor.

Let us consider high frequency monochromatic EM wave of the form:

$$\begin{cases} \mathcal{E}(\mathbf{x}, t) = E(\mathbf{x})e^{-i\omega t} \\ \mathcal{D}(\mathbf{x}, t) = D(\mathbf{x})e^{-i\omega t} \\ \mathcal{H}(\mathbf{x}, t) = H(\mathbf{x})e^{-i\omega t} \\ \mathcal{B}(\mathbf{x}, t) = B(\mathbf{x})e^{-i\omega t}. \end{cases} \quad (2.3.3)$$

where $\omega \gg 1$ is the frequency. In addition, we assume

$$\varepsilon = \varepsilon_0 \delta + \frac{1}{k_0} f. \quad (2.3.4)$$

where ε_0 is a constant, $k_0 = \omega/c \gg 1$ is the wave number and f is a second order symmetric tensor. This assumption, which is called **quasi-isotropic**, assumes that the photoelastic material is approximately isotropic and homogeneous, and the stress-induced part

of permittivity is relatively small. On the other hand, since most photoelastic materials are non-magnetic, we assume

$$\mu = \delta. \quad (2.3.5)$$

Introducing (2.3.3)(2.3.4)(2.3.5) into (2.3.1), we get

$$\begin{cases} \nabla \times H + ik_0(\varepsilon_0\delta + \frac{1}{k_0}f)E & = 0 \\ \nabla \times E - ik_0H & = 0. \end{cases} \quad (2.3.6)$$

For a quasi-isotropic material, it is natural to consider the WKB approximation. The ansatz is

$$\begin{cases} E(\mathbf{x}) & = e^{ik_0\tau(\mathbf{x})} \sum_{m \geq 0} \frac{E^{(m)}(\mathbf{x})}{(ik_0)^m} \\ H(\mathbf{x}) & = e^{ik_0\tau(\mathbf{x})} \sum_{m \geq 0} \frac{H^{(m)}(\mathbf{x})}{(ik_0)^m}, \end{cases} \quad (2.3.7)$$

where $\tau(x)$ is a phase function. By introducing (2.3.7), we can decompose (2.3.6) into an infinite system of equations by equating the coefficients of the same powers of the wave number k_0 on both sides.

$$\begin{cases} H^{(m)} \times \nabla\tau + \nabla \times H^{(m-1)} + \varepsilon_0 E^{(m)} + if E^{(m-1)} & = 0 \\ E^{(m)} \times \nabla\tau + \nabla \times E^{(m-1)} - H^{(m)} & = 0 \end{cases} \quad (2.3.8)$$

for $m = 0, 1, \dots$. Here we define $E^{(-1)} = H^{(-1)} = 0$ for convenience.

Let's start from $m = 0$ to find $H^{(0)}$ and $E^{(0)}$,

$$\begin{cases} H^{(0)} \times \nabla\tau + \varepsilon_0 E^{(0)} & = 0 \\ E^{(0)} \times \nabla\tau - H^{(0)} & = 0. \end{cases} \quad (2.3.9)$$

Solving these two equations gives

$$\langle E^{(0)}, \nabla\tau \rangle \nabla\tau + (\varepsilon_0 - |\nabla\tau|^2) E^{(0)} = 0. \quad (2.3.10)$$

By taking the inner product of (2.3.10) with $\nabla\tau$, we obtain

$$\langle E^{(0)}, \nabla\tau \rangle = 0, \quad (2.3.11)$$

since $\varepsilon_0 \neq 0$. With this result, (2.3.10) now takes the form

$$(\varepsilon_0 - |\nabla\tau|^2) E^{(0)} = 0. \quad (2.3.12)$$

Thus, the phase function τ must satisfy the eikonal equation:

$$|\nabla\tau|^2 = n_0^2 := \varepsilon_0 \quad (2.3.13)$$

where n_0 is the refractive index.

To solve the eikonal equations, we use geometric optics approximation by assuming the solution is a plane wave

$$\tau(\mathbf{x}) = n_0 \mathbf{x} \cdot \xi, \quad (2.3.14)$$

where $\xi \in \mathbb{S}^2$ is the propagating direction of the wave and the straight lines in the direction ξ are called rays. With this, (2.3.9) becomes

$$\begin{cases} H^{(0)} \times \xi + n_0 E^{(0)} = 0 \\ n_0 E^{(0)} \times \xi - H^{(0)} = 0. \end{cases} \quad (2.3.15)$$

Therefore, order zero WKB approximation leads to that ξ , $E^{(0)}$ and $H^{(0)}$ are perpendicular to each other.

Next, consider the case $m = 1$ in (2.3.8). Using (2.3.14), we get

$$\begin{cases} n_0 H^{(1)} \times \xi + \nabla \times H^{(0)} + \varepsilon_0 E^{(1)} + if E^{(0)} = 0 \\ n_0 E^{(1)} \times \xi + \nabla \times E^{(0)} - H^{(1)} = 0. \end{cases} \quad (2.3.16)$$

Using (2.3.15), we arrive

$$(n_0^2 E^{(1)} \cdot \xi + n_0 \nabla \cdot E^{(0)}) \xi - n_0 \frac{\partial E^{(0)}}{\partial \xi} + if E^{(0)} = 0. \quad (2.3.17)$$

Here, $\partial E / \partial \xi$ denotes the direction derivative $\xi \cdot \nabla E$. We may decompose this vector equation into the ray direction ξ and its perpendicular ξ^\perp . First, we notice that

$$\frac{\partial E}{\partial \xi} \in \xi^\perp. \quad (2.3.18)$$

This is due to the fact that $\langle \xi, E \rangle = 0$ along the ray. Let $\pi_\xi := \delta - \xi\xi^T$, the projection in \mathbb{R}^3 onto ξ^\perp . For any 2-tensor f , the projection $\pi_\xi(fE^{(0)})$ for $E^{(0)} \in \xi^\perp$ can be re-expressed as $P_\xi(f)E^{(0)}$, where $P_\xi(f) := \pi_\xi f \pi_\xi$. With these, the projection of the above vector equation onto ξ^\perp reads

$$\frac{\partial E^{(0)}}{\partial \xi} = \frac{i}{n_0} P_\xi f E^{(0)}, \quad (2.3.19)$$

and the corresponding approximate solution is

$$\mathcal{E}(\mathbf{x}, t) \approx e^{i(k_0 n_0 \mathbf{x} \cdot \xi - \omega t)} E^{(0)}(\mathbf{x}). \quad (2.3.20)$$

Here, we only keep $E^{(0)}$ in the WKB approximation (2.3.7) since $k_0 \gg 0$. From now on, we simply denote $E^{(0)}$ by E .

Remark 2.1. Let $A = |\mathcal{E}|^2 = E^* E$, then

$$\begin{aligned} \frac{\partial A}{\partial \xi} &= \frac{\partial E^*}{\partial \xi} E + E^* \frac{\partial E}{\partial \xi} \\ &= \frac{-i}{n_0} E^* (P_\xi f)^* E + \frac{i}{n_0} E^* P_\xi f E \\ &= 0 \end{aligned} \quad (2.3.21)$$

since $P_\xi f$ is symmetric.

This means when the wave is propagating in the media, its amplitude does not change; the property quasi-isotropy casue only a retardation on the phase of the wave.

2.4 Transverse Ray Transform

Let us consider a photoelastic object in \mathbb{R}^3 . When a high frequency monochromatic light, e.g. laser, passes through it, the change of polarization is governed by (2.3.19). This ODE gives us a forward imaging model for such a photoelastic object. We shall integrate this ODE below. To do so, let $\gamma : [0, l] \rightarrow \mathbb{R}^3$ be a ray in the direction ξ passing the object and be parametrized by $\tau \in [0, l]$. Let us abbreviate the field $E(\gamma(\tau))$ by $E(\tau)$. The ODE above for E along the ray can be rewritten as

$$\frac{dE}{d\tau} = \frac{i}{n_0} P_\xi f E. \quad (2.4.1)$$

We first assume $E(l)$ is just some linear transform of $E(0)$

$$E(l) = UE(0) \quad (2.4.2)$$

where the linear transformation U is depend on f on γ . Follow [2], $U(\gamma)$ can be expanded via Peano-Baker series

$$\begin{aligned} U &= I + \int_0^l A(\tau_1) d\tau_1 + \int_0^l A(\tau_1) \int_0^{\tau_1} A(\tau_2) d\tau_2 d\tau_1 + \dots \\ &= I + \sum_{n=1}^{\infty} \mathcal{I}_n \end{aligned} \quad (2.4.3)$$

where

$$A(\tau) = (i/n_0)P_{\xi}f(\tau). \quad (2.4.4)$$

We simplify this by using only $I + \mathcal{I}_1$ to approximate U ,¹ i.e.

$$U \approx I + \frac{i}{n_0} \int_0^l P_{\xi}f(\tau) d\tau. \quad (2.4.5)$$

The forward model becomes

$$E(l) = \left(I + \frac{i}{n_0} \int_0^l P_{\xi}f(\tau) d\tau \right) E(0). \quad (2.4.6)$$

The consequence above shows that if we detect the object by a ray along γ , then the change of polarization is

$$\int_{\gamma} P_{\xi}f(\tau) d\tau, \quad (2.4.7)$$

which is a useful information to reconstruct f .

Similar to the approach in radiative CT, we introduce the following ray transform. First, any ray in \mathbb{R}^3 in the direction ξ can be identified as a point (ξ, \mathbf{x}) in the tangent plane of S^2 at ξ .

Definition 2.1. *The transverse ray transform (TRT) $J : \mathcal{S}(\mathbb{R}^3; S^2\mathbb{R}^3) \rightarrow \mathcal{S}(TS^2; S^2\mathbb{R}^3)$ is defined by*

$$Jf(\xi, \mathbf{x}) := \int_{-\infty}^{\infty} P_{\xi}f(\mathbf{x} + t\xi) dt. \quad (2.4.8)$$

The imaging process of integrated photoelasticity can be regarded as collecting the TRT data of f to reconstruct f .

¹Actually, we need $n_0 \gg 1$ here.

2.5 The Polarization Ellipse

To get TRT of f , we must first determine U from detecting $E(0)$ and $E(l)$. In following two sections, we will examine its feasibility in practice.

Let $\{\mathbf{e}_1, \mathbf{e}_2, \mathbf{e}_3\}$ be an orthonormal basis of \mathbb{R}^3 . Let us consider the ray direction $\xi = \mathbf{e}_3$. We can decompose E into

$$E(\tau) = E_1(\tau)\mathbf{e}_1 + E_2(\tau)\mathbf{e}_2 \quad (2.5.1)$$

and (2.3.19) becomes,

$$\begin{cases} \frac{dE_1}{d\tau} = \frac{i}{n_0} (f_{11}E_1 + f_{12}E_2) \\ \frac{dE_2}{d\tau} = \frac{i}{n_0} (f_{21}E_1 + f_{22}E_2) \end{cases} \quad (2.5.2)$$

where f_{jk} is the representation of f w.r.t. the orthonormal basis $\{\mathbf{e}_1, \mathbf{e}_2, \mathbf{e}_3\}$.

\mathcal{E} and E are both complex. It is the real vector

$$\eta(\tau, t) = \text{Re } \mathcal{E} = \text{Re} [E(\tau)e^{i(k_0 n_0 \tau - \omega t)}] \quad (2.5.3)$$

that has a physical meaning. One can check that, for fix $\tau = \tau_0$, the vectors

$$\eta(\tau_0, t) = \text{Re} [(E_1(\tau_0)\mathbf{e}_1 + E_2(\tau_0)\mathbf{e}_2)e^{i(k_0 n_0 \tau_0 - \omega t)}], t \in \mathbb{R} \quad (2.5.4)$$

form an ellipse on the plane perpendicular to $\mathbf{e}_3 = \xi$. It is called the polarization ellipse, see Figure 2.6. Let $\mathbf{u}_1, \mathbf{u}_2$ be the direction axes of the polarization ellipse, and let λ be the angle between \mathbf{u}_1 and \mathbf{e}_1 . Then we have

$$\begin{cases} \mathbf{u}_1 = \mathbf{e}_1 \cos \lambda + \mathbf{e}_2 \sin \lambda \\ \mathbf{u}_2 = -\mathbf{e}_1 \sin \lambda + \mathbf{e}_2 \cos \lambda. \end{cases} \quad (2.5.5)$$

Let a, b be the semiaxes of the ellipse w.r.t. \mathbf{u}_1 and \mathbf{u}_2 , respectively, then

$$\eta(\tau_0, t) = a \cos(\phi_0 - \omega t)\mathbf{u}_1 \pm b \sin(\phi_0 - \omega t)\mathbf{u}_2 = \text{Re} [(a\mathbf{u}_1 \mp ib\mathbf{u}_2)e^{i(\phi_0 - \omega t)}], \quad (2.5.6)$$

where the choice of sign in this equality depends on the motion (2.5.4) is clockwise or counterclockwise. Inserting (2.5.5) into the equation above, we get

$$\eta(\tau_0, t) = \text{Re} [(a \cos \lambda \pm ib \sin \lambda)\mathbf{e}_1 + (a \sin \lambda \mp ib \cos \lambda)\mathbf{e}_2]e^{i(\phi_0 - \omega t)} \quad (2.5.7)$$

Comparing (2.5.4) and (2.5.7), we then have

$$\begin{cases} E_1(\tau_0) = (a \cos \lambda \pm ib \sin \lambda)e^{i(\phi_0 - k_0 n_0 \tau_0)} \\ E_2(\tau_0) = (a \sin \lambda \mp ib \cos \lambda)e^{i(\phi_0 - k_0 n_0 \tau_0)} \end{cases} \quad (2.5.8)$$

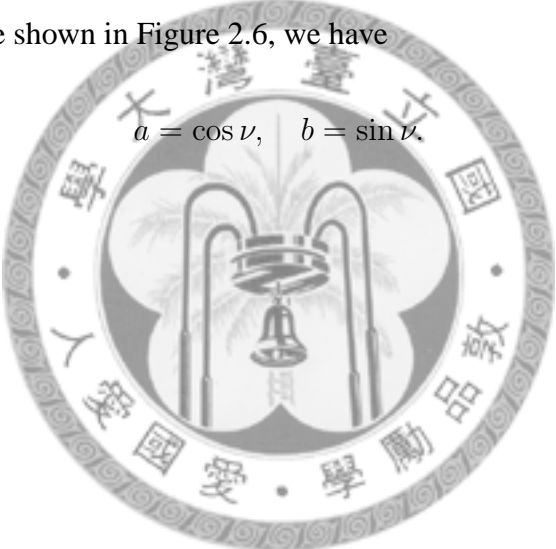
From remark 2.1, we can assume that

$$|E_1(\tau)|^2 + |E_2(\tau)|^2 = \|E(0)\|^2 = 1. \quad (2.5.9)$$

From (2.5.6), this is equivalent to

$$a^2 + b^2 = 1. \quad (2.5.10)$$

If we let ν be the angle shown in Figure 2.6, we have

$$a = \cos \nu, \quad b = \sin \nu. \quad (2.5.11)$$


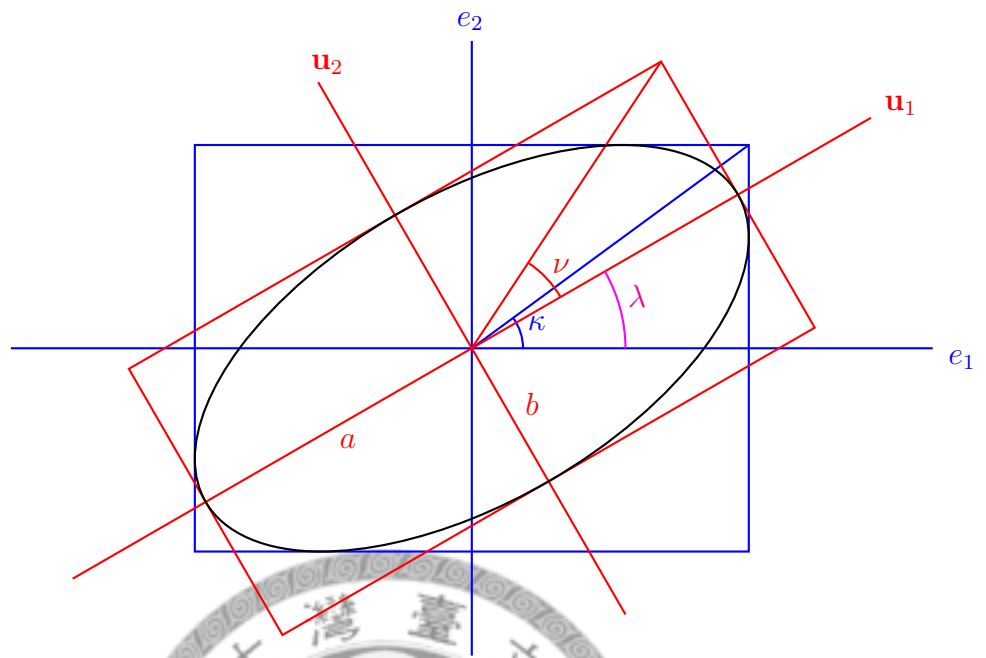


Figure 2.6: Polarization Ellipse



2.6 Truncated Transverse Ray Transform

We have just shown the polarization ellipse is determined by three angles, i.e. λ , ν and $(\phi_0 - k_0 n_0 \tau_0)$, and E is determined by (2.5.8) and (2.5.11) accordingly. If we rewrite (2.4.2) in coordinate form w.r.t. $\{\mathbf{e}_1, \mathbf{e}_2, \mathbf{e}_3\}$

$$\begin{pmatrix} E^1(l) \\ E^2(l) \end{pmatrix} = \begin{pmatrix} U_{11} & U_{12} \\ U_{21} & U_{22} \end{pmatrix} \begin{pmatrix} E^1(0) \\ E^2(0) \end{pmatrix}, \quad (2.6.1)$$

we will find that the number of unknowns is three (since U is symmetric), and the information given by the polarization ellipse is sufficient to determine U . However, in practice, only λ and ν can be got easily; it is difficult to detect the phase information $(\phi_0 - k_0 n_0 \tau_0)$. This is actually an underdetermined problem, and for that, we need to make some compromise.

Consider a vector field \tilde{E} along γ defined by

$$\tilde{E}(\tau) = E(\tau) \cdot \exp \left[\frac{i}{2n_0} \int_0^\tau (f_{11} + f_{22}) \right], \quad (2.6.2)$$

for the polarization ellipse, the corresponding $\tilde{\lambda}$ and $\tilde{\nu}$ are equal to λ and ν , respectively. \tilde{E} satisfies a similar ODE as (2.5.2)

$$\begin{cases} \frac{d\tilde{E}_1}{d\tau} = \frac{i}{n_0} \left[\frac{1}{2}(f_{11} - f_{22})\tilde{E}_1 + f_{12}\tilde{E}_2 \right] \\ \frac{d\tilde{E}_2}{d\tau} = \frac{i}{n_0} \left[f_{21}\tilde{E}_1 + \frac{1}{2}(f_{22} - f_{11})\tilde{E}_2 \right], \end{cases} \quad (2.6.3)$$

or equivalently,

$$\frac{d\tilde{E}}{d\tau} = \frac{i}{n_0} Q_\xi f \quad (2.6.4)$$

where the operator Q_ξ is defined by

$$Q_\xi f = P_\xi f - \frac{1}{2} \text{tr}(P_\xi f) \pi_\xi. \quad (2.6.5)$$

Apply Peano-Baker series again, we have

$$\tilde{E}(l) = V\tilde{E}(0) \quad (2.6.6)$$

where

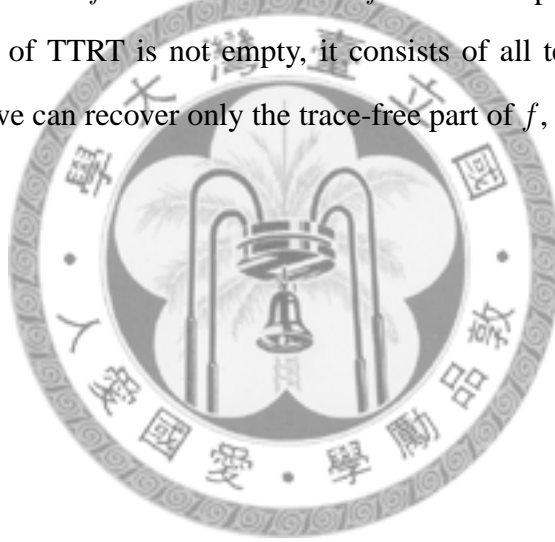
$$V \approx I + \frac{i}{n_0} \int_0^l Q_\xi f(\tau) d\tau. \quad (2.6.7)$$

Here we made another definition

Definition 2.2. *The truncated transverse ray transform (TTRT) $K : \mathcal{S}(\mathbb{R}^3; S^2\mathbb{R}^3) \rightarrow \mathcal{S}(T\mathbb{S}^2; S^2\mathbb{R}^3)$ is defined by*

$$Kf(\xi, \mathbf{x}) := \int_{-\infty}^{\infty} Q_\xi f(\mathbf{x} + t\xi) dt. \quad (2.6.8)$$

Because of the missing information in integrated photoelasticity, the imaging data we get is actually TTRT of f instead of TRT of f . This compromise, however, has a drawback: the kernel of TTRT is not empty, it consists of all tensor field of the form $a(\mathbf{x})\delta$. As the result, we can recover only the trace-free part of f , i.e. $f - \text{tr}(f)\delta/3$.



Chapter 3

Reconstruction Methods

According the model we derived in the previous chapter, let us reformulate the reconstruction problem of integrated photoelasticity:

Problem 3.1 (Invert TTRT).

Given $L \subset TS^2$ and $g \in \mathcal{S}(L; S^2\mathbb{R}^3)$, find a trace-free tensor field $f \in \mathcal{S}(\mathbb{R}^3; S^2\mathbb{R}^3)$ such that

$$Kf|_L = g. \quad (3.0.1)$$

The reason why we consider a subset L of TS^2 is because

$$\dim(TS^2) = 4 > 3 = \dim(\mathbb{R}^3). \quad (3.0.2)$$

Therefore, the reconstruction may need only partial data of TTRT. On the other hand, the trace-free condition is due to the degeneracy of K . In the following discussion, we assume f is trace-free unless otherwise stated.

3.1 Aben's method

In [1], the author derived a reconstruction method based on physical assumption that there is no external forces apply on the detecting object, and it is in equilibrium.

Suppose the detecting object is put in \mathbb{R}^3 and consider a thin slice ABC , where these three point are on the boundary of the object, and set the coordinate according to Figure 3.1. Let rays pass through the slice along the direction y' on the upper and lower surfaces,

whose coordinates are z_u and z_l , respectively. We then get the data

$$\begin{cases} K_l^1(s) &= C \int_{x'=s, z=z_l} (\sigma_{x'x'} - \sigma_{zz}) dy' \\ K_l^2(s) &= C \int_{x'=s, z=z_l} \sigma_{x'z} dy' \end{cases} \quad (3.1.1)$$

$$\begin{cases} K_u^1(s) &= C \int_{x'=s, z=z_u} (\sigma_{x'x'} - \sigma_{zz}) dy' \\ K_u^2(s) &= C \int_{x'=s, z=z_u} \sigma_{x'z} dy', \end{cases} \quad (3.1.2)$$

where σ represents the stress; this uses stress-optic law stated in (2.1.1). Use the physical assumption mentioned in the beginning, when Δz is close to zero, we have

$$\Delta z \int_A^C \sigma_{x'x'} dy' = T_u - T_l \quad (3.1.3)$$

where T_u and T_l are the shear forces on the upper and lower surfaces of the slice, respectively, which can be formulated by

$$\begin{cases} T_u &= \frac{1}{C} \int_d^B K_u^2(s) ds \\ T_l &= \frac{1}{C} \int_d^B K_l^2(s) ds \end{cases} \quad (3.1.4)$$

Combine these results and let $\Delta z \rightarrow 0$, we reach the result

$$\int_A^C \sigma_{zz} dy' = \frac{1}{C} \frac{d}{dz} \int_d^B K_2 dx' - K_1. \quad (3.1.5)$$

Rotate the coordinate (x', y') , we obtain Radon transform of σ_{zz} .

To summarize, Aben's method let us determine the Radon transform of each component of f from Kf . We then use Radon inversion techniques to reconstruct f .

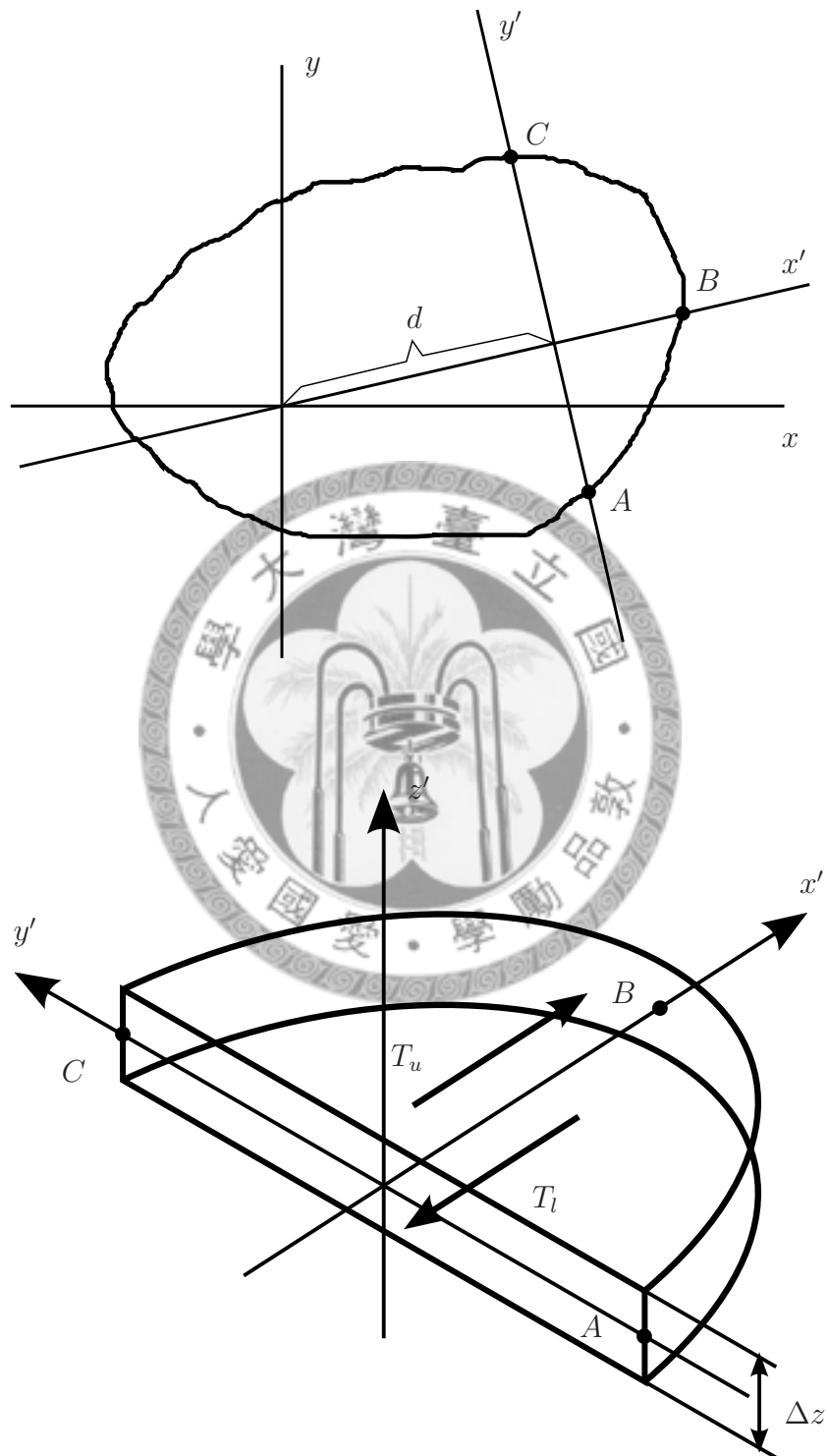


Figure 3.1: Aben's Method

3.2 Sharafutdinov's Methods

In [6], the author propose another reconstruction method by Fourier transform.

First, we rewrite $Q_\xi f$ to its coordinate form

$$(Q_\xi f)_{ij} = f_{ij} - \frac{1}{|\xi|^2}(f_{ip}\xi_p\xi_j + f_{jp}\xi_p\xi_i) + \frac{1}{2|\xi|^4}f_{pq}\xi_p\xi_q\xi_i\xi_j + \frac{1}{|\xi|^2}f_{pq}\xi_p\xi_q\delta_{ij}. \quad (3.2.1)$$

Here is an example: suppose $\xi = e_3$ then

$$\begin{aligned} (Q_\xi f)_{ij} &= f_{ij} - (f_{i3}\delta_{j3} + f_{j3}\delta_{i3}) + \frac{1}{2}f_{33}\delta_{i3}\delta_{j3} + \frac{1}{2}f_{33}\delta_{ij} \\ &= \begin{pmatrix} \frac{1}{2}(f_{11} - f_{22}) & f_{12} & 0 \\ f_{21} & \frac{1}{2}(f_{22} - f_{11}) & 0 \\ 0 & 0 & 0 \end{pmatrix} \end{aligned}$$

We make a definition

Definition 3.1. *The back projection operator*

$$\mu : C^\infty(\mathbb{R}^3 \times \mathbb{R}_0^3; S^2\mathbb{R}^3) \rightarrow C^\infty(\mathbb{R}^3; S^2\mathbb{R}^3) \quad (3.2.2)$$

is defined by

$$\mu\phi(x) = \frac{1}{4\pi} \int_{S^2} \phi(x, \xi) d\omega(\xi), \quad (3.2.3)$$

The composition $\mu K : \mathcal{S}(\mathbb{R}^3; S^2\mathbb{R}^3) \rightarrow C^\infty(\mathbb{R}^3; S^2\mathbb{R}^3)$ can be written as

$$\mu K f = B_1 f + B_2 f + B_3 f + B_4 f, \quad (3.2.4)$$

where

$$\begin{cases} B_1 f &= \frac{1}{2\pi} f * |x|^{-2}, \\ (B_2 f)_{ij} &= -\frac{1}{2\pi} (f_{ik} * \frac{x_j x_k}{|x|^4} + f_{jk} * \frac{x_i x_k}{|x|^4}), \\ (B_3 f)_{ij} &= \frac{1}{4\pi} f_{kl} * \frac{x_i x_j x_k x_l}{|x|^6}, \\ (B_4 f)_{ij} &= \frac{1}{4\pi} f_{kl} * \frac{x_k x_l}{|x|^4} \delta_{ij}. \end{cases} \quad (3.2.5)$$

If we denote $h = (2/\pi)\mu K f$ and apply the Fourier transform on it, we have

$$\hat{f}_{ij} - \frac{1}{2}(\hat{f}_{ik}\epsilon_{jk} + \hat{f}_{jk}\epsilon_{ik}) + \frac{3}{16}\hat{f}_{kl}\epsilon_{ij}^2 + \frac{1}{4}\hat{f}_{kl}\epsilon_{kl}\delta_{ij} = |y|\hat{h}_{ij} \quad (3.2.6)$$

where $e_i = y_i/|y|$ and $\epsilon_{ij} = \delta_{ij} - e_i e_j$. Here is a lemma

Lemma 3.1. *If the right-hand side of (3.2.6) meets the condition $j\hat{h} = 0$, then the system of equations has a unique solution satisfying the condition $j\hat{f} = 0$, and the solution can be expressed as*

$$\hat{f}_{ij} = 2|y| \left[4\hat{h}_{ij} - 3 \left(\hat{h}_{ik}e_k e_j + \hat{h}_{jk}e_k e_i \right) + \hat{h}_{kl}e_k e_l e_i e_j + \frac{5}{3}\hat{h}_{kl}e_k e_l \delta_{ij} \right]. \quad (3.2.7)$$

The result can be also written in invariant form

$$\hat{f}(y) = 2|y| \left(4 - \frac{6}{|y|^2} i_y j_y + \frac{1}{|y|^4} i_y^2 j_y^2 + \frac{5}{3} \frac{1}{|y|^2} i_y j_y^2 \right) \hat{h}(y). \quad (3.2.8)$$

Apply the Fourier inversion we reach the result

$$f = \frac{4}{\pi} (-\Delta)^{1/2} \left(4 - 6\Delta^{-1} d\delta + \Delta^{-2} d^2 \delta^2 + \frac{5}{3} i\Delta^{-1} \delta^2 \right) \mu K f. \quad (3.2.9)$$

For the detail of this reconstruction method, please refer to section 6 in [6].

This formula, which involves a 3 dimensional back projection, needs full information of TTRT to reconstruct the tensor field f , therefore, may not be good for practical usage.

3.3 Lioheart and Sharafutdinov's Method

In [4], the authors proposed a reconstruction method similar to previous one, but use partial data of TTRT only.

The subset L mentioned in the beginning of this chapter is chosen as follows:

$$\begin{cases} L_\eta &= \{(\xi, x) \in T\mathbb{S}^2 \mid \langle \xi, \eta \rangle = 0\} \quad \text{for } \eta \in \mathbb{S}^2 \\ L &= \bigcup_{j=1}^N L_{\eta_j}. \end{cases} \quad (3.3.1)$$

Briefly speaking, by choosing N directions $\{\eta_j\}_{j=1}^N$, we collect TTRT data only by rays perpendicular to one of these directions.

The idea of this reconstruction method is as follows: Consider the data $g|_{L_\eta}$ for a given unit vector η . For a plane P perpendicular to η , the restriction of the vector field $\eta \times f(x)\eta$ can be considered as a 2D vector field on P . On the other hand, we consider the slice tensor of f is a second order tensor field on P . We then apply a slice-by-slice reconstruction to these vector and tensor fields on each plane. The reconstruction procedure is similar to classical reconstruction method of inverting 2D Radon transform. The

result under the Fourier space can be written as

$$\begin{cases} \Phi_\eta(y)\hat{f}(y) &= \lambda_\eta(y) \\ \Psi_\eta(y)\hat{f}(y) &= \mu_\eta(y), \end{cases} \quad (3.3.2)$$

where λ_η and μ_η can be obtain from TTRT data, and this indicate that the recontruction problem is merely to solve algebraic equations in Fourier space.

3.3.1 Logitudinal Ray Transform (LRT)

We introduce another kind of ray transform here,

Definition 3.2 (Logitudinal Ray Transform (LRT)).

The logitudinal ray transform (LRT)

$$I : \mathcal{S}(\mathbb{R}^3; S^n \mathbb{C}^3) \rightarrow \mathcal{S}(T\mathbb{S}^2) \quad (3.3.3)$$

is defined by

$$If(\xi, \mathbf{x}) = \int_{-\infty}^{\infty} \langle f(\mathbf{x} + t\xi), \xi^n \rangle dt. \quad (3.3.4)$$

LRT is a transformation which applies on any order of tensor field. It is noteworthy that when $n = 0$, LRT is just the ordinary ray transform defined on \mathbb{R}^3 . In this section, we use only cases $n = 1$ and $n = 2$.

LRT can be also defined on a tensor field on a plane in \mathbb{R}^3 .

Definition 3.3 (LRT on a Plane).

For an $\eta \in \mathbb{S}^2$, let $\eta^\perp = \{\xi \in \mathbb{R}^3 \mid \langle \xi, \eta \rangle = 0\}$, $S^n \eta^\perp$ be the complex order n tensor field on η^\perp , and $\mathbb{S}_\eta^1 = \{\xi \in \eta^\perp \mid |\xi| = 1\}$ be the unit sphere in ξ^\perp . Given $s \in \mathbb{R}$, let $s\eta + \eta^\perp$ be a plane pass through $s\eta$ and perpendicular to η . The LRT on the plane $s\eta + \eta^\perp$

$$I_{\eta,s} : \mathcal{S}(s\eta + \eta^\perp; S^n \eta^\perp) \rightarrow \mathcal{S}(T\mathbb{S}_\eta^1) \quad (3.3.5)$$

is defined by

$$I_{\eta,s}f(\xi, x) := \int_{-\infty}^{\infty} \langle f(s\eta + x + t\xi^n), \xi \rangle dt. \quad (3.3.6)$$

The relation between these two definition is as follows:

$$I_{\eta,s}(\iota_{\eta,s}^* f)(\xi, x) = If(\xi, s\eta + x) \quad (3.3.7)$$

where $\iota_{\eta,s} : \mathcal{S}(s\eta + \eta^\perp; S^n \eta^\perp) \subset \mathcal{S}(\mathbb{R}^3; S^n \mathbb{C}^3)$ is the embedding of a tensor field and $\iota_{\eta,s}^*$ is its conjugate. The relation of LRT and TTRT can be described by the following lemma:

Lemma 3.2. *Let $f \in \mathcal{S}(\mathbb{R}^3; S^2 \mathbb{C}^3)$ be a trace free tensor field. Equations*

$$\begin{cases} I_{\eta,s}((\eta \times f\eta)|_{s\eta+\eta^\perp}) &= K_{\eta,s}^1 f, \\ I_{\eta,s}(\iota_{\eta,s}^* f - 2\text{tr}(\iota_{\eta,s}^* f)\delta) &= 2K_{\eta,s}^2 f \end{cases} \quad (3.3.8)$$

hold for every $s \in \mathbb{R}$ and $\eta \in \mathbb{S}^2$, where the functions $K_{\eta,s}^i f \in \mathcal{S}(T\mathbb{S}_\eta^1)$ ($i = 1, 2$) are defined by

$$\begin{cases} (K_{\eta,s}^1 f)(\xi, x) &= \langle (Kf)(\xi, s\eta + x)\eta, \xi \times \eta \rangle, \\ (K_{\eta,s}^2 f)(\xi, x) &= \langle (Kf)(\xi, s\eta + x)\eta, \eta \rangle. \end{cases} \quad (3.3.9)$$

Since for each ray, the TTRT contains two independent components, the conversion from TTRT to LRT is without any loss of information in 3.3.8. Next, we need to find the inversion formula for LRT in order the reconstruct f . For any details of this lemma, please refer to [4].

3.3.2 Inversion Formula of LRT

We make a definition first.

Definition 3.4 (Tengential Component).

For a vector field $g \in C^\infty(\mathbb{R}^2; \mathbb{C}^2)$, we define its tengential component $\tau g \in C^\infty(\mathbb{R}^2)$ by

$$(\tau g)(y) = \langle g(y), y^\perp \rangle, \quad (3.3.10)$$

where the vector y^\perp is obtained by rotating y by $\pi/2$.

For a tensor field $g \in C^\infty(\mathbb{R}^2; S^2 \mathbb{C}^2)$, we define its tengential component $\tau g \in C^\infty(\mathbb{R}^2)$ by

$$(\tau g)(y) = |y|^2 \text{tr}(g) - \langle g(y)y, y \rangle. \quad (3.3.11)$$

And we have the following inversion formula for LRT

Lemma 3.3 (Inverseion Formula of LRT).

For a vector field $f \in \mathcal{S}(\mathbb{R}^2; \mathbb{C}^2)$, the tangential component of its Fourier transform $\mathcal{F}[f]$ can be recovered from its LRT by the formula

$$\tau \mathcal{F}[f] = \frac{i}{2} |y| \mathcal{F} \left[B \left(\frac{\partial(I f)}{\partial p} \right) \right]. \quad (3.3.12)$$

For a tensor field $f \in \mathcal{S}(\mathbb{R}^2; S^2 \mathbb{C}^2)$, the tangential component of its Fourier transform $\mathcal{F}[f]$ can be recovered from its LRT by the formula

$$\tau \mathcal{F}[f] = \frac{1}{2} |y|^3 \mathcal{F}[B(I f)]. \quad (3.3.13)$$

Here $B : \mathcal{S}(TS^1) \rightarrow C^\infty(\mathbb{R}^2)$ is the two dimensional back projection operator, and the Fourier transform is defined componentwisely.

For details of LRT, please refer to chapter 2 of [6].

3.3.3 Algebraic Equations in Fourier Space

Combining Lemma 3.2 and 3.3, (3.3.2) can be written explicitly:

Lemma 3.4. Let \hat{f} be the 3D Fourier transform of a trace free tensor field $f \in \mathcal{S}(\mathbb{R}^3; S^2 \mathbb{C}^3)$.

For a unit vector $\eta \in \mathbb{S}^2$, equations

$$\begin{cases} \langle \hat{f}(y) \eta, \pi_\eta y \rangle & = \lambda_\eta(y) \\ |\pi_\eta y|^2 \langle \hat{f}(y) \eta, \eta \rangle - \langle \hat{f}(y) \pi_\eta y, \pi_\eta y \rangle & = \mu_\eta(y) \end{cases} \quad (3.3.14)$$

hold on \mathbb{R}^3 with RHS defined by

$$\begin{cases} \lambda_\eta(y) & = \frac{i}{2} |\pi_\eta y| \mathcal{F}_{x \rightarrow y} \left[\left(B_\eta \frac{\partial(K_\eta^1 f)}{\partial p} \right) (x) \right], \\ \mu_\eta(y) & = |\pi_\eta y|^3 \mathcal{F}_{x \rightarrow y} [(B_\eta K_\eta^2 f)(x)]. \end{cases} \quad (3.3.15)$$

where K_η^j ($j = 1, 2$) is define in (3.3.9).

By choosing a direction η and collect the TTRT data on L_η , we than have two linear equations of $\hat{f}_{ij}(y)$ for each $y \in \mathbb{R}^3$. In a symmetric trace free tensor, there are five known, therefore, it seems that we need only three directions to reconstruct f .

In [4], the authors prove that choosing

$$\begin{cases} \eta_1 = \mathbf{e}_1, \\ \eta_2 = \mathbf{e}_2, \\ \eta_3 = \mathbf{e}_3 \end{cases} \quad (3.3.16)$$

is sufficient for solving \hat{f} , but unstable, since the linear system degenerate at $y_i = 0$ for any $i = 1, 2, 3$. We can still use the continuity of \hat{f} to determined its value in these point.

By choosing six direction:

$$\begin{cases} \eta_1 = (\mathbf{e}_2 + \mathbf{e}_3)/\sqrt{2}, & \eta_2 = (\mathbf{e}_3 + \mathbf{e}_1)/\sqrt{2}, & \eta_3 = (\mathbf{e}_1 + \mathbf{e}_2)/\sqrt{2}, \\ \eta_4 = (\mathbf{e}_2 - \mathbf{e}_3)/\sqrt{2}, & \eta_5 = (\mathbf{e}_3 - \mathbf{e}_1)/\sqrt{2}, & \eta_6 = (\mathbf{e}_1 - \mathbf{e}_2)/\sqrt{2}, \end{cases} \quad (3.3.17)$$

we can get a stable reconstruction of \hat{f} , with the stability estimate

$$\begin{cases} |\hat{f}(y)| & \leq C \left(|y|^{-1} \sum_{i=1}^6 |\lambda_i(y)| + |y|^{-2} \sum_{i=1}^3 |\mu_i(y) - \mu_{i+3}(y)| \right) \\ |\hat{f}(y)|^2 & \leq C'' \left(|y|^{-2} \sum_{i=1}^6 |\lambda_i(y)|^2 + |y|^{-4} \sum_{i=1}^3 |\mu_i(y) - \mu_{i+3}(y)|^2 \right) \end{cases} \quad (3.3.18)$$

This method has advantages over the previous two. First, it did not need the assumption that the object is in equilibrium and can use to determine its residual stress. And second, it uses only partial data of TTRT.

In this paper, however, we do not follow any of these reconstruction method. We'll use the algebraic reconstruction techniques and applied TV regularization via augmented Lagrangian method and see whether an acceptable result can be obtained.

Chapter 4

Augmented Lagrangian Method

Reduce this problem to its fundamentals, the reconstruction problem is just solving a linear system, $Kf = g$, where we consider the partial TTRT data g is as in (3.3.1). This problem is equivalent to an L2 minimization problem:

$$\min\{\|Kf - g\|^2\}. \quad (4.0.1)$$

If K is non-degenerate, the minimizer is just the solution of $Kf = g$. Here we want to add TV regularization into this minimization scheme and find the minimizer by iterative method. There are two consideration for us to do so: first, for practical applications, noise is inevitable, therefore, g may not be in the range of K ; second, for ordinary ray transform, it has high frequency singular vectors corresponding to small singular values. It may be the same for TTRT, and if it is true, gradient descent method in L2 minimization scheme may have a slow convergence rate for the high frequency parts; TV regularization would improve this situation.

In this chapter, We propose a numerical reconstruction in TV-L2 scheme using algebraic reconstruction method and augmented lagrangian method.

4.1 Augmented Lagrangian Method

Consider the constraint problem

$$\min f(\mathbf{x}) \quad \text{subject to} \quad c(\mathbf{x}) = 0. \quad (4.1.1)$$

The ordinary penalty method use the following unconstraint iterative approach

$$\mathbf{x}_k = \min\{\Psi_k(\mathbf{x}) = f(\mathbf{x}) + \mu_k |c(\mathbf{x})|^2\} \quad (4.1.2)$$

To find the minimizer in the equation above, we can use gradient descent method. We use larger μ_k after each iteration to ensure the final result will satisfy the constraint.

The augmented Lagrangian method use the following unconstraint iterative approach instead

$$\mathbf{x}_k = \min\{L_k(\mathbf{x}) = f(\mathbf{x}) + \mu_k |c(\mathbf{x})|^2 - \lambda c(\mathbf{x})\}. \quad (4.1.3)$$

After each iteration, in addition to updating μ_k , the variable λ is also updated by

$$\lambda \leftarrow \lambda - \mu_k c(\mathbf{x}_k) \quad (4.1.4)$$

In ordinary penalty approach, when μ_k becomes larger and larger, its convergence rate would becomes slower and slower. For augmented Lagrangian method, the additional linear term can help \mathbf{x}_k converges to a solution satisfies given constraint without letting μ_k go to infinity. It improves the rate of convergence.

4.2 Alternating Direction Method

To solve the reconstruction problem in interated photoelasticity, We apply *Alternating Direction Method (ADM)* in [10] which is based on augmented Lagrangian method.

We denote the TV functional of the tensor field by $\Phi(f)$, where the TV norm of a tensor field is defined by adding TV norm for each components of the tensor field. A basic TV-L2 minimization scheme, which is also known as ROF model, is

$$\min_f \{\alpha \Phi(f) + \frac{1}{2} \|Kf - g\|_2^2\}. \quad (4.2.1)$$

However, since Φ is non-differetiable, use gradient descent method directly may have a slow convergence rate. Hence, we introduce some auxiliary variable w to be the gradient of tensor f , then the minimization problem can be rewrite as a constraint minization problem

$$\min_{f,w} \{\alpha \|w\|_1 + \frac{1}{2} \|Kf - g\|_2^2\} \quad \text{subject to} \quad \nabla f = w. \quad (4.2.2)$$

The augmented Lagrangian function of (4.2.2) is

$$\mathcal{L}(f, w) = \alpha(\|w\|_1 - \langle \lambda, w - \nabla f \rangle) + \frac{\beta}{2} \|w - \nabla f\|_2^2 + \frac{1}{2} \|Kf - g\|_2^2. \quad (4.2.3)$$

In discretized scheme, suppose the voxel is indexed by $n = 1, 2, \dots, N$, the formula above becomes

$$\mathcal{L}(f, w) = \alpha \left(\sum_{i,j,n} \|w_{i,j}^n\| - \sum_{i,j,n} \lambda_{i,j}^n \cdot (w - \nabla f)_{i,j}^n + \frac{\beta}{2} \|w - \nabla f\|_2^2 \right) + \frac{1}{2} \|Kf - g\|_2^2. \quad (4.2.4)$$

where $w_{i,j}^n$ is a 3-d vector for each $i, j = 1, 2, 3, n = 1, \dots, N$ and ∇ is the discretized gradient.

Our goal is to find the minimizer of \mathcal{L} , and this can be done by minimizing it w.r.t. f and w alternately.

We minimize \mathcal{L} w.r.t. f by gradient descent method, i.e.

$$f^{k+1} = f^k - \Delta t \left(-\alpha(\nabla \cdot \lambda^k) + \alpha\beta \nabla \cdot (w^{k+1} - \nabla f^k) + K^*(Kf^k - g) \right) \quad (4.2.5)$$

On the other hand, minimization of \mathcal{L} w.r.t. w can be done by the following formula

$$(w^{k+1})_{i,j}^n = s((\nabla f^k + \lambda/\beta)_{i,j}^n, 1/\beta). \quad (4.2.6)$$

where $s(\xi, 1/\beta)$, known as the 3-dimensional soft-thresholding, is defined as

$$s(\xi, 1/\beta) = \max\{\|\xi\| - 1/\beta, 0\} \frac{\xi}{\|\xi\|}. \quad (4.2.7)$$

We summarize this method to the following algorithm

Algorithm 4.1 (ADM).

Require: $f^0, \lambda^0, M, \Delta t$

$$f = f^0, \lambda = \lambda^0$$

for $k = 0 \rightarrow M - 1$ **do**

$$w_{ij}^n \leftarrow s((\nabla f + \lambda/\beta)_{ij}^n, 1/\beta)$$

$$f \leftarrow f - \Delta t(-\alpha(\nabla \cdot \lambda) + \alpha\beta \nabla \cdot (w - \nabla f) + K^*(Kf - g))$$

$$\lambda \leftarrow \lambda - \beta(w - \nabla f)$$

end for

Here we just set a large number of iterations and record its result. We test this algorithm on the partial TTRT data of 3, 6, and 9 directions.

Chapter 5

Numerical Results

5.1 Numerical Settings

The test subject we choose is a 50-by-50-by-50 tensor phantom, which is tracefree and piecewise constant, see the figure 5.1.

In our numerical experiments, we'll make two comparisons: one is between between ADM in TV-L2 scheme and gradient descent method in L2 scheme. This comparison shows whether TV regularization has any advantages.

Another is among three different sets of TTRT data. These three sets of TTRT data are different in η 's they choose in (3.3.1): one is with three η 's as in (3.3.16); one is with six η 's as in (3.3.17); the last is with nine η 's by combining the previous two. In [4], the authors have already shown it is sufficient to reconstruct f by (3.3.16), and the reconstruction is stable with (3.3.17). We want to know whether and how more TTRT data would improve the reconstruction.

For each slice, the TTRT data is collected by 75 rays for each angle and 90 angles uniformly distributed in $[0, \pi]$.

5.2 Results

First, we will show the result reconstructed by gradient descent method in L2 scheme with differet number of η 's.

The result of 3 η 's is shown in Figure 5.2.

The result of 6 η 's is shown in Figure 5.3.

The result of 9 η 's is shown in Figure 5.4.

Next, we will show the result reconstructed by ADM in TV-L2 scheme with different number of η 's. For regularization parameters, we choose $\alpha = 0.1, \beta = 1000$.

The result of 3 η 's is shown in Figure 5.5.

The result of 6 η 's is shown in Figure 5.6.

The result of 9 η 's is shown in Figure 5.7.

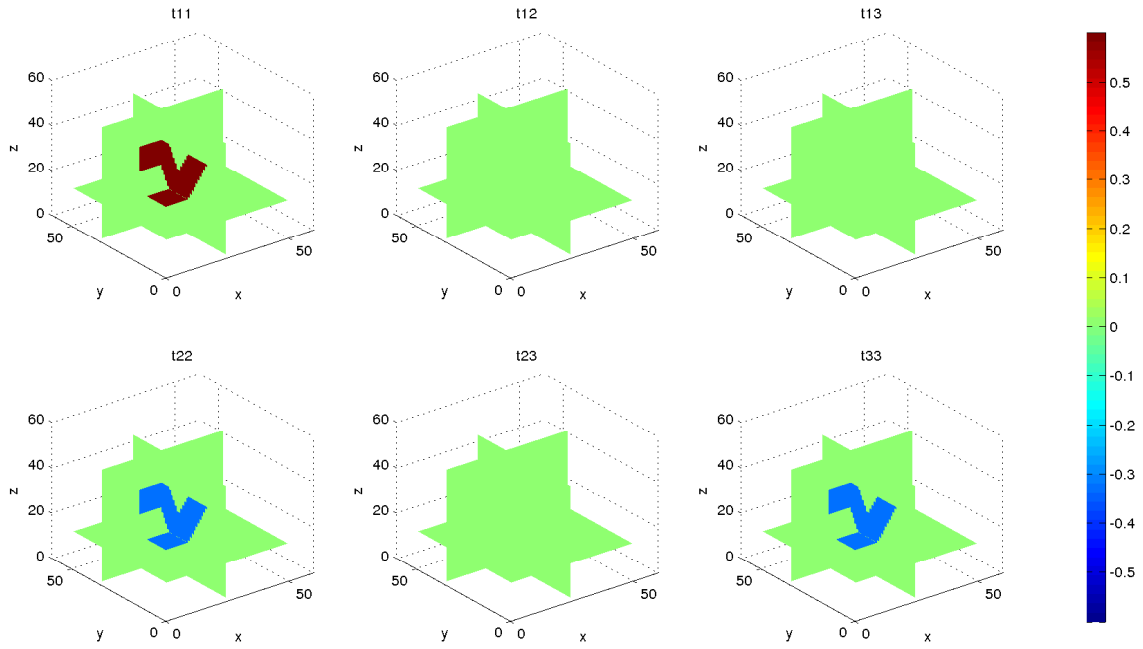
At the end, we will compare the decreasing of relative errors of these methods, which are measured in l2 sense.

For gradient descent method, comparison among 3, 6, 9 η 's is shown in Figure 5.8.

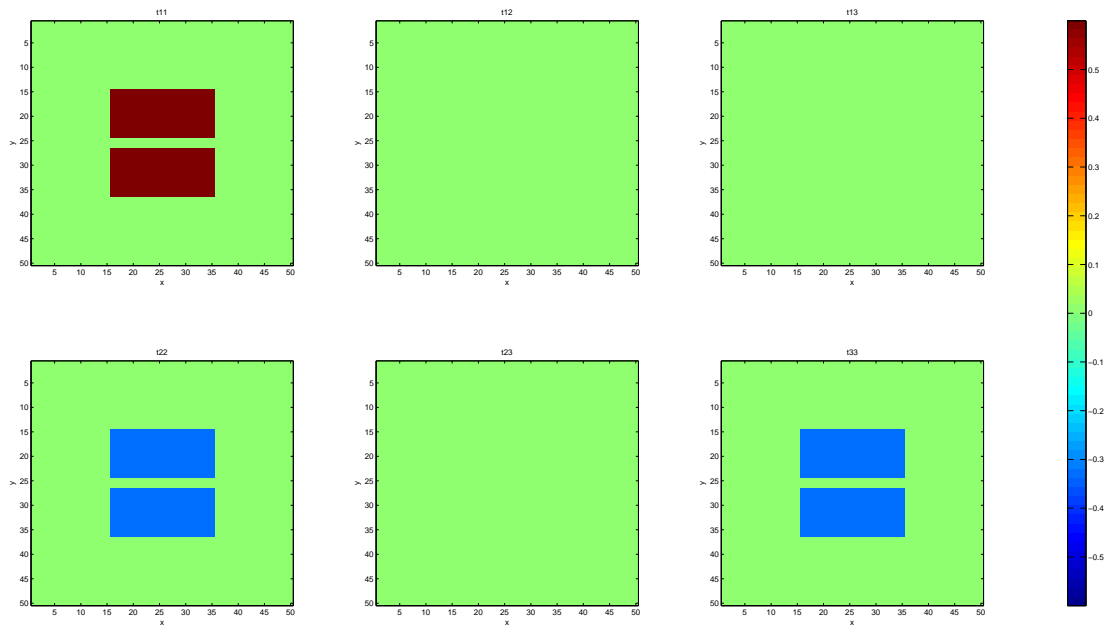
For ADM, comparison among 3, 6, 9 η 's is shown in Figure 5.9.

Comparison between gradient descent method and ADM with different η 's is shown in Figure 5.10 and 5.11 and 5.12.



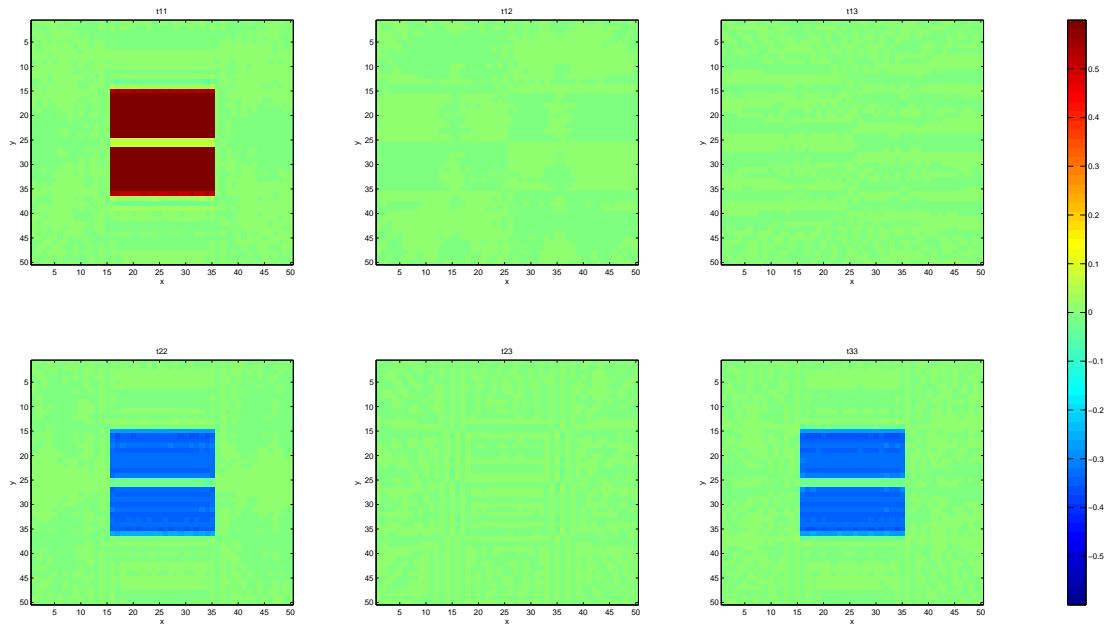
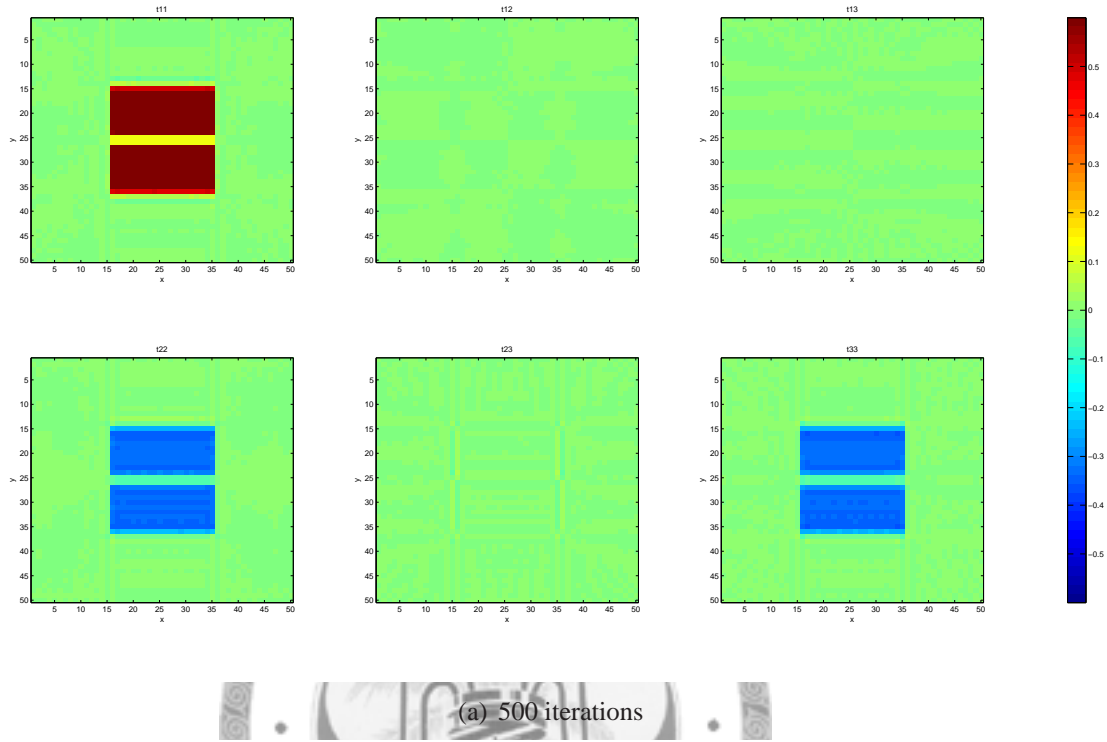


(a) Volumetric Slice Plot



(b) Slice Plot at $z = 27$

Figure 5.1: Testing Tensor Phantom



(b) 1000 iterations

Figure 5.2: Reconstruction by gradient descent method with 3 η 's.

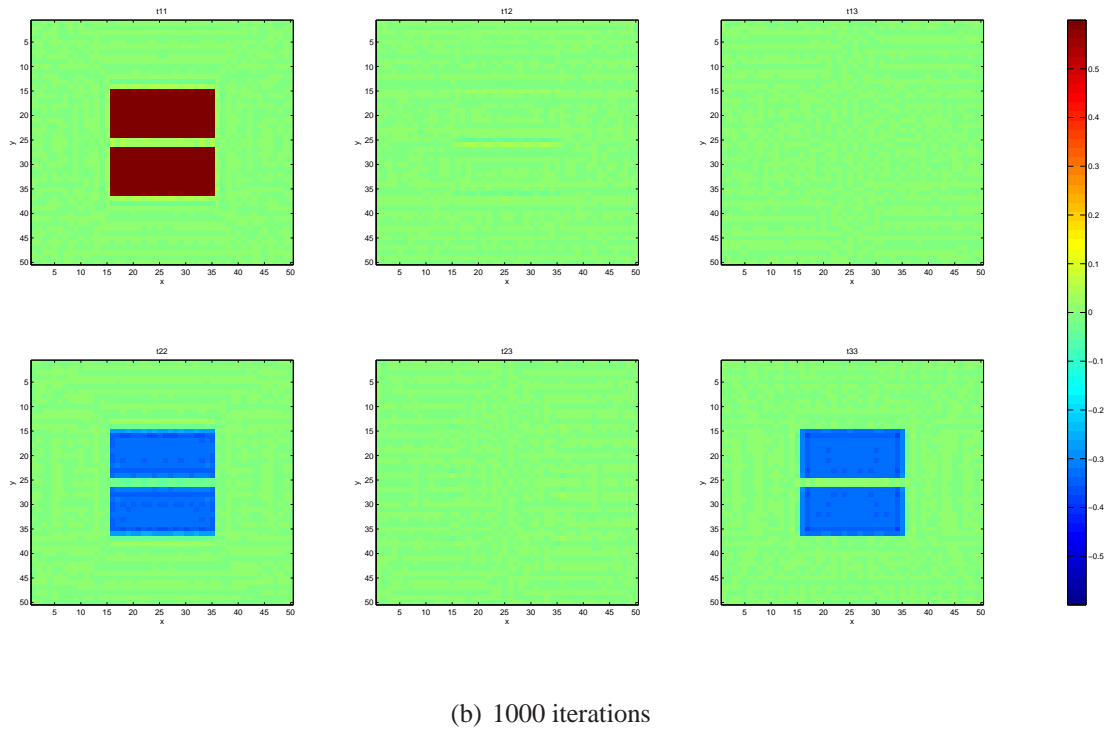
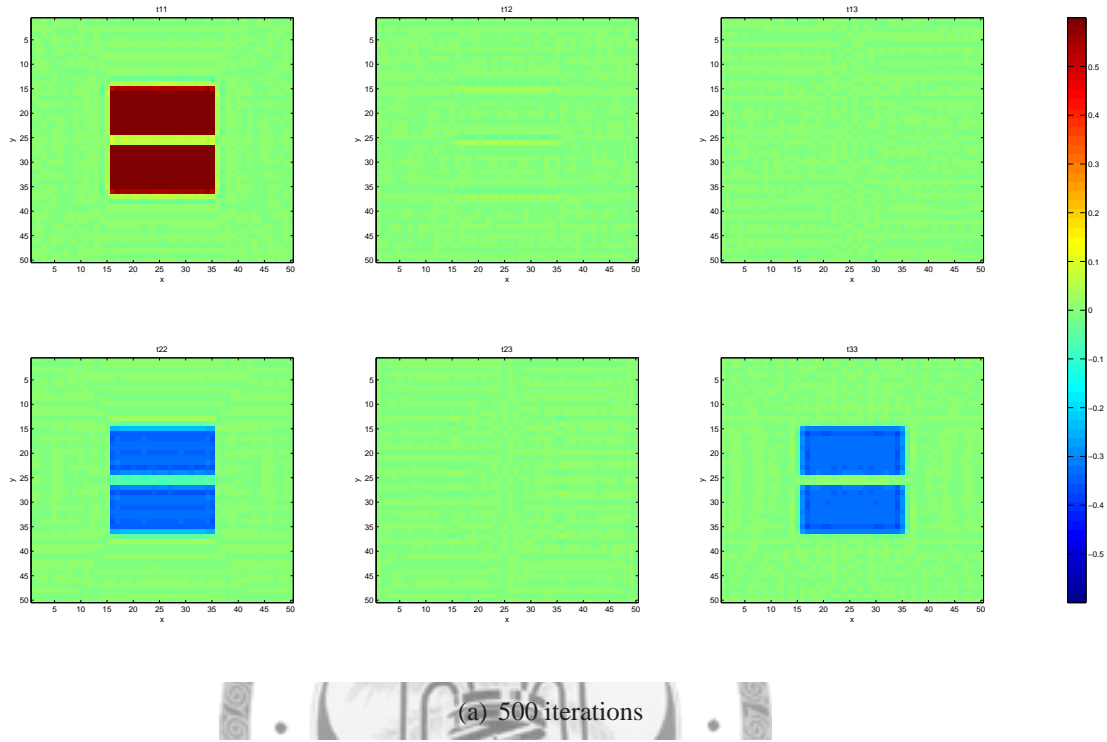
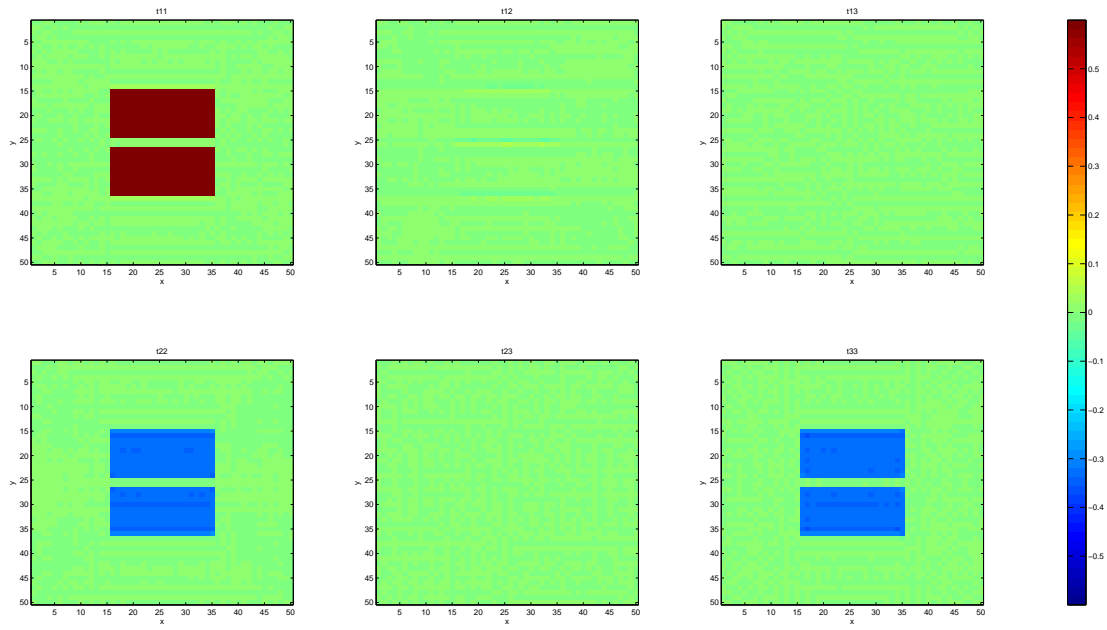
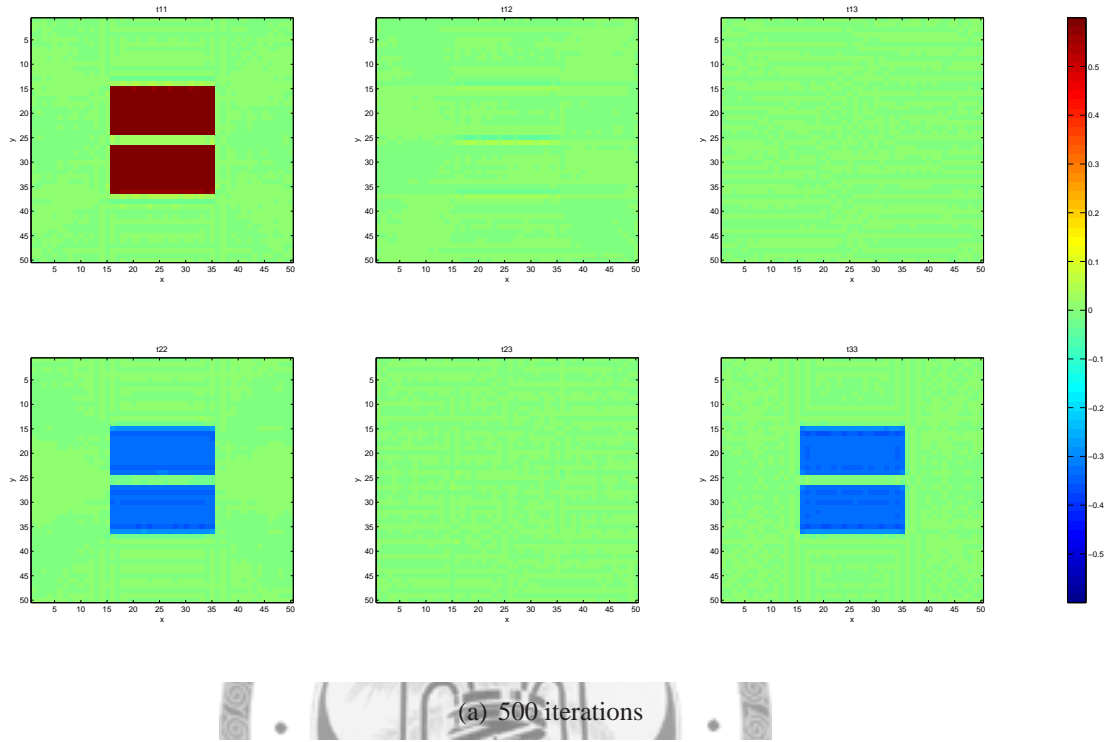
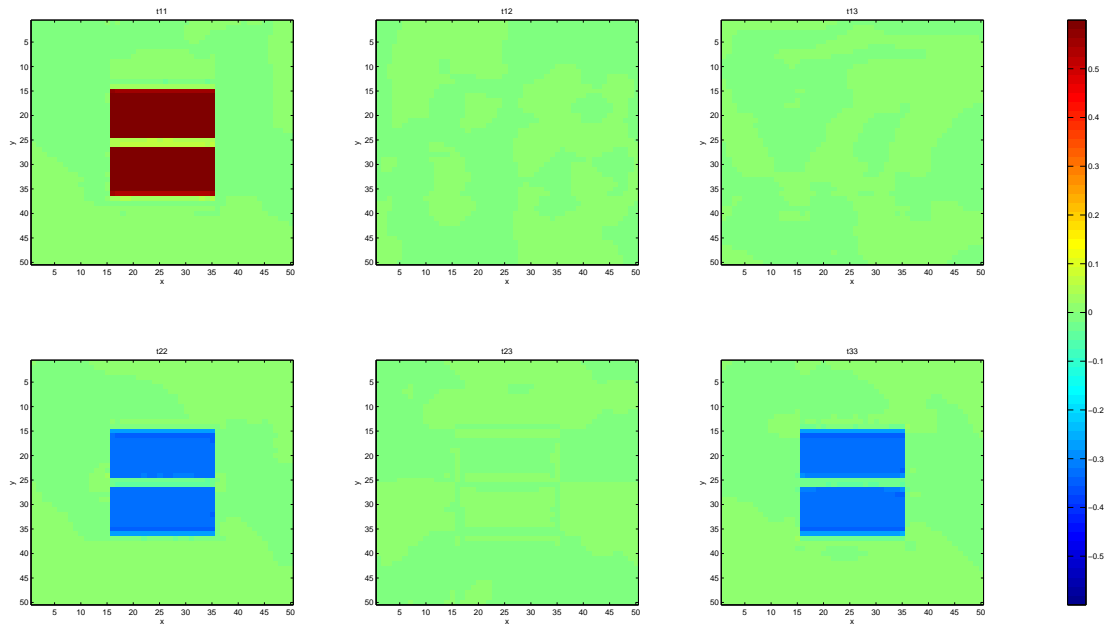
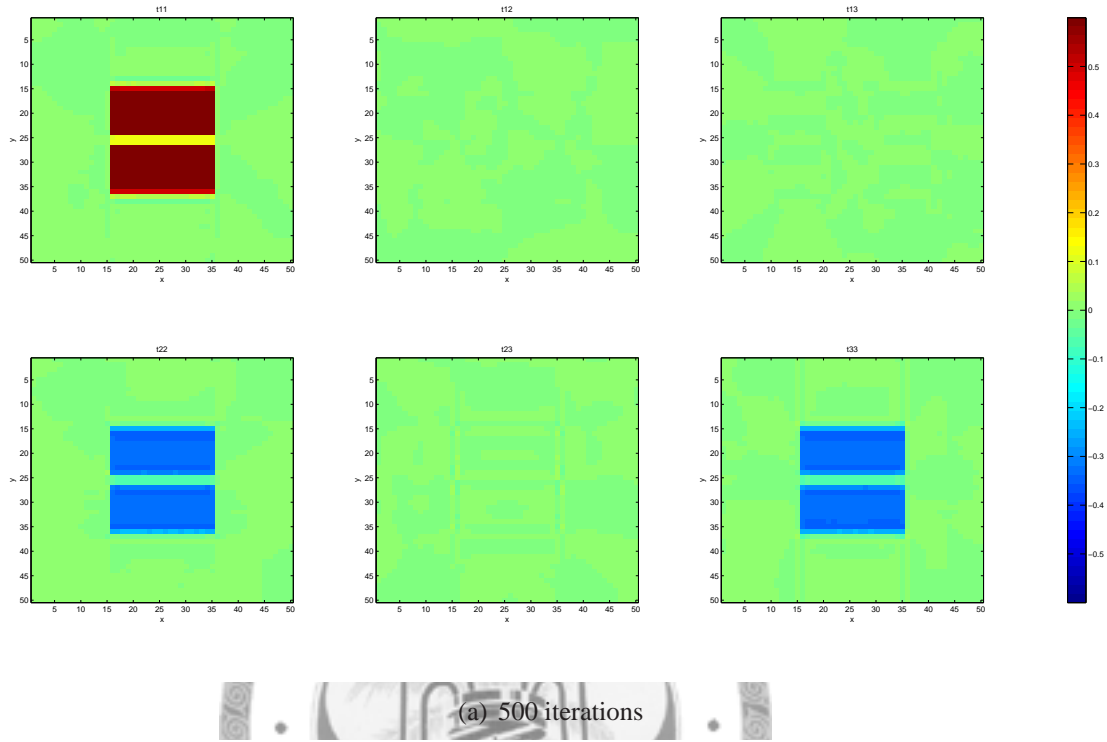


Figure 5.3: Reconstruction by gradient descent method with 6 η 's.



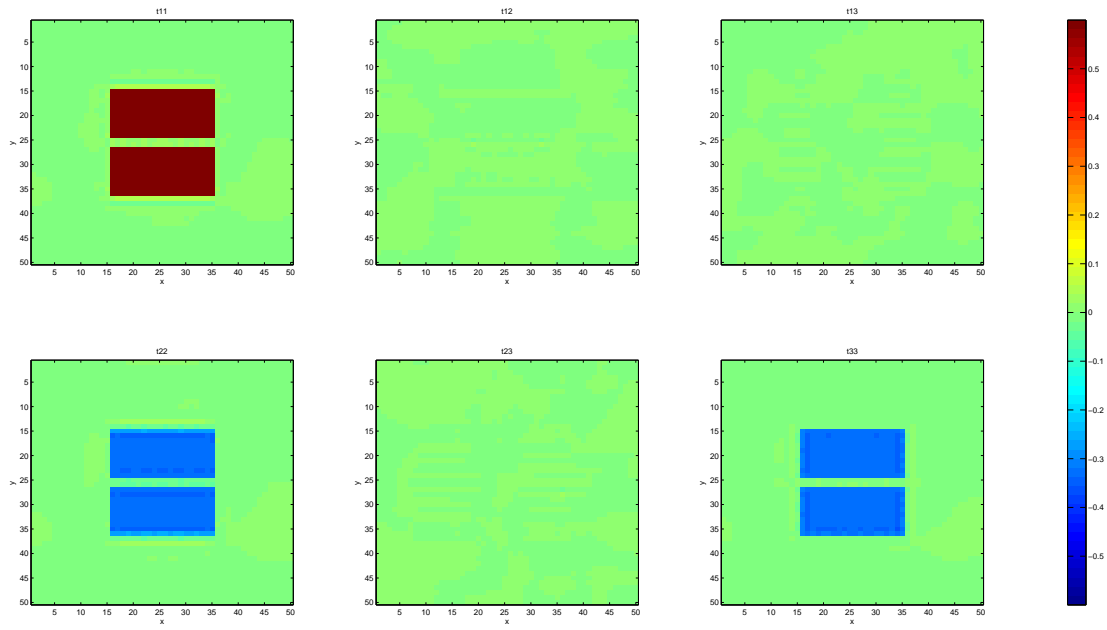
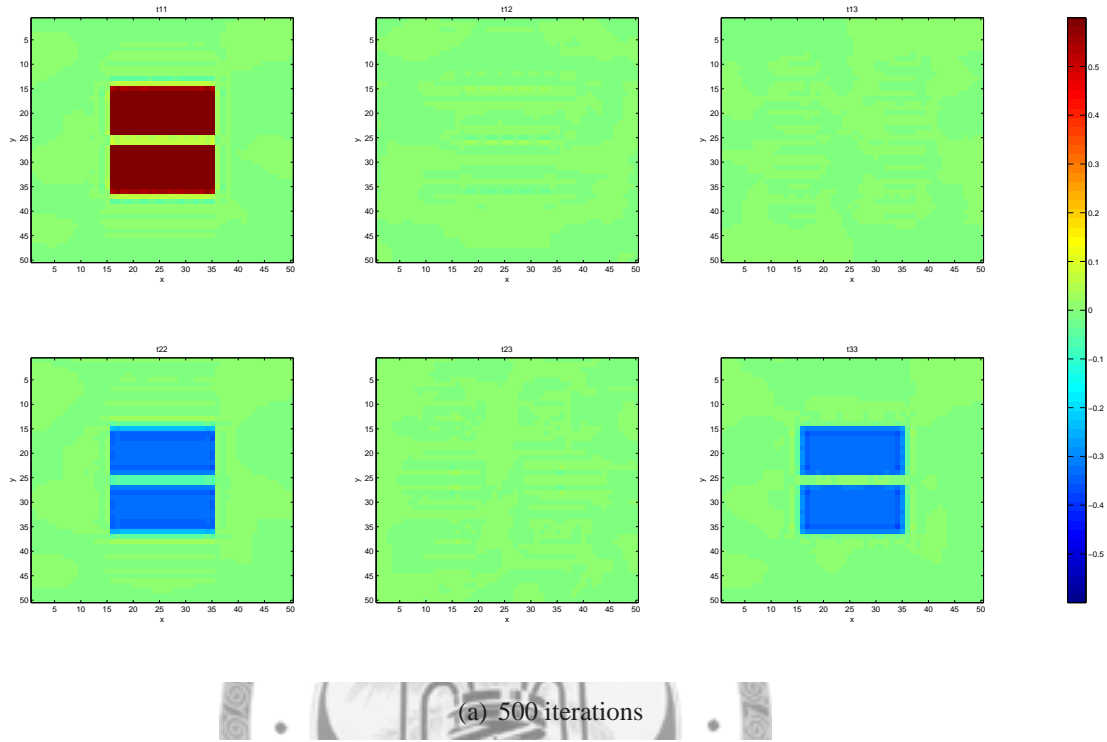
(b) 1000 iterations

Figure 5.4: Reconstruction by gradient descent method with 9 η 's.



(b) 1000 iterations

Figure 5.5: Reconstruction by ADM with 3 η 's.



(b) 1000 iterations

Figure 5.6: Reconstruction by ADM with 6 η 's.

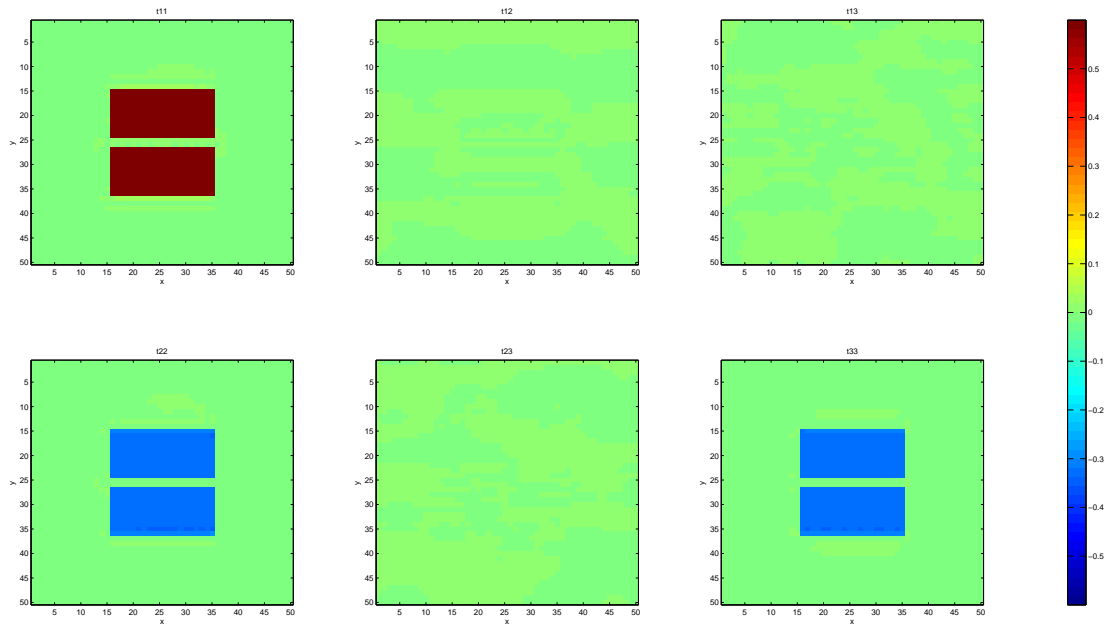
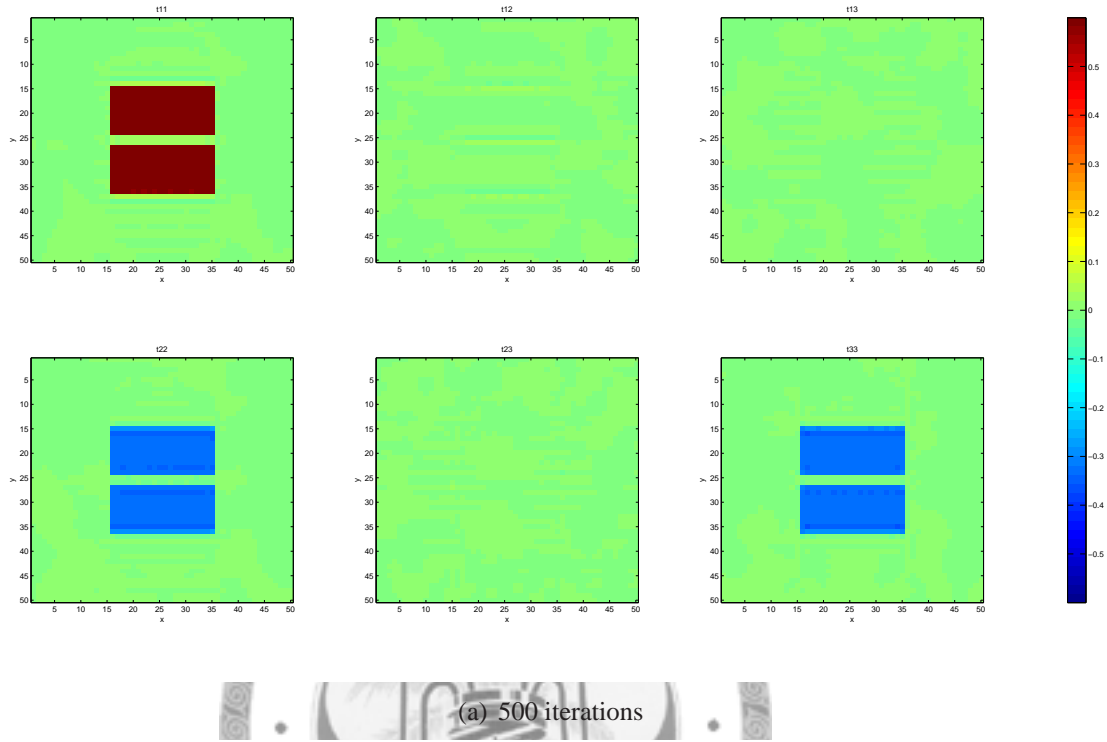


Figure 5.7: Reconstruction by ADM with 9 η 's.

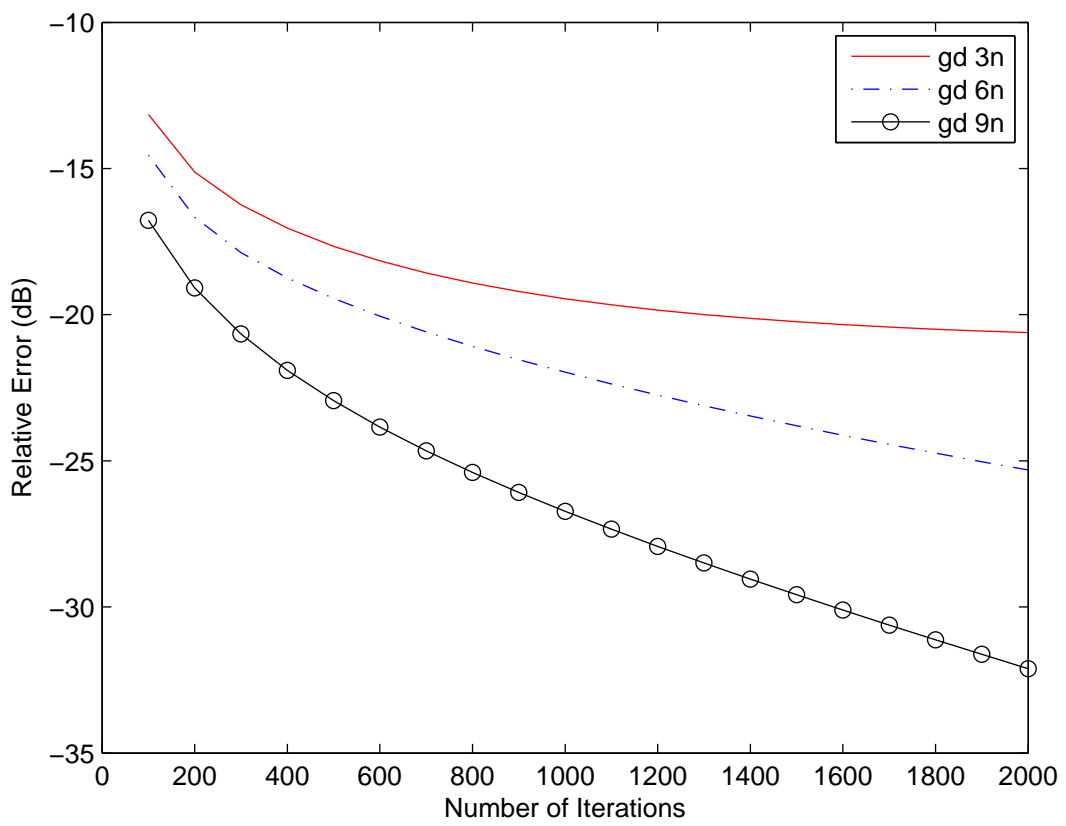


Figure 5.8: Comparison among different number of η 's for gradient descent method.

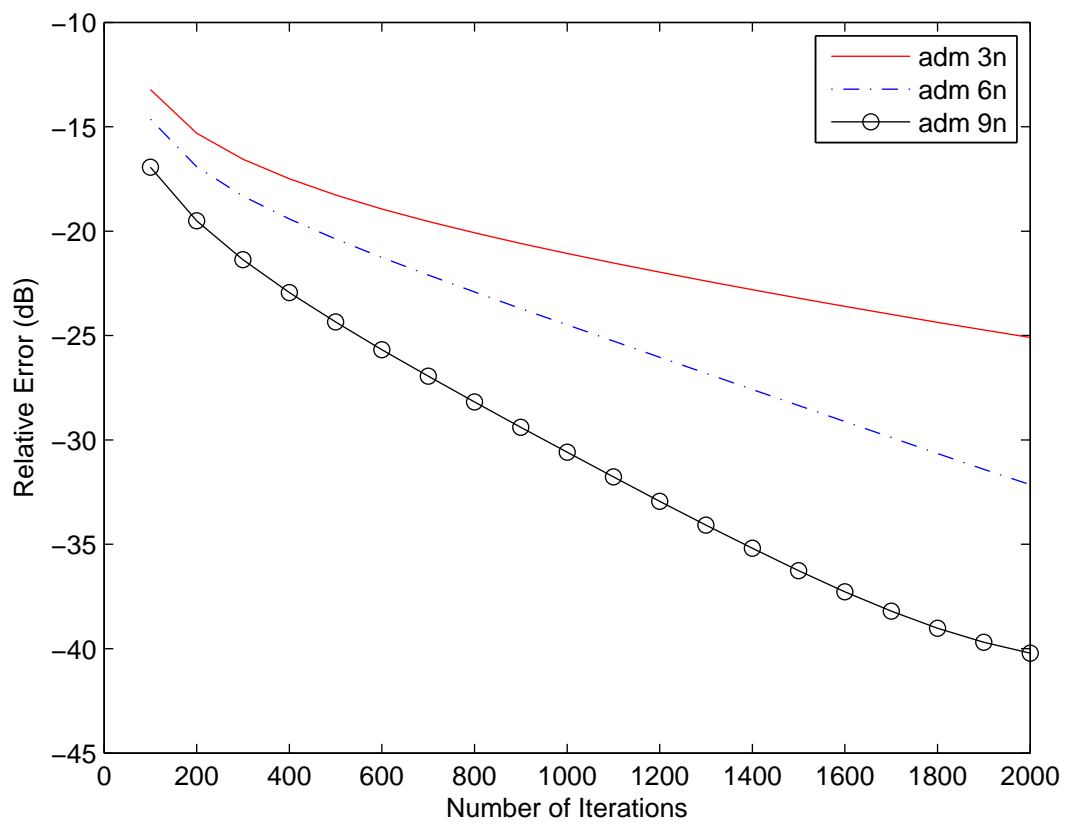


Figure 5.9: Comparison among different number of η 's for ADM.

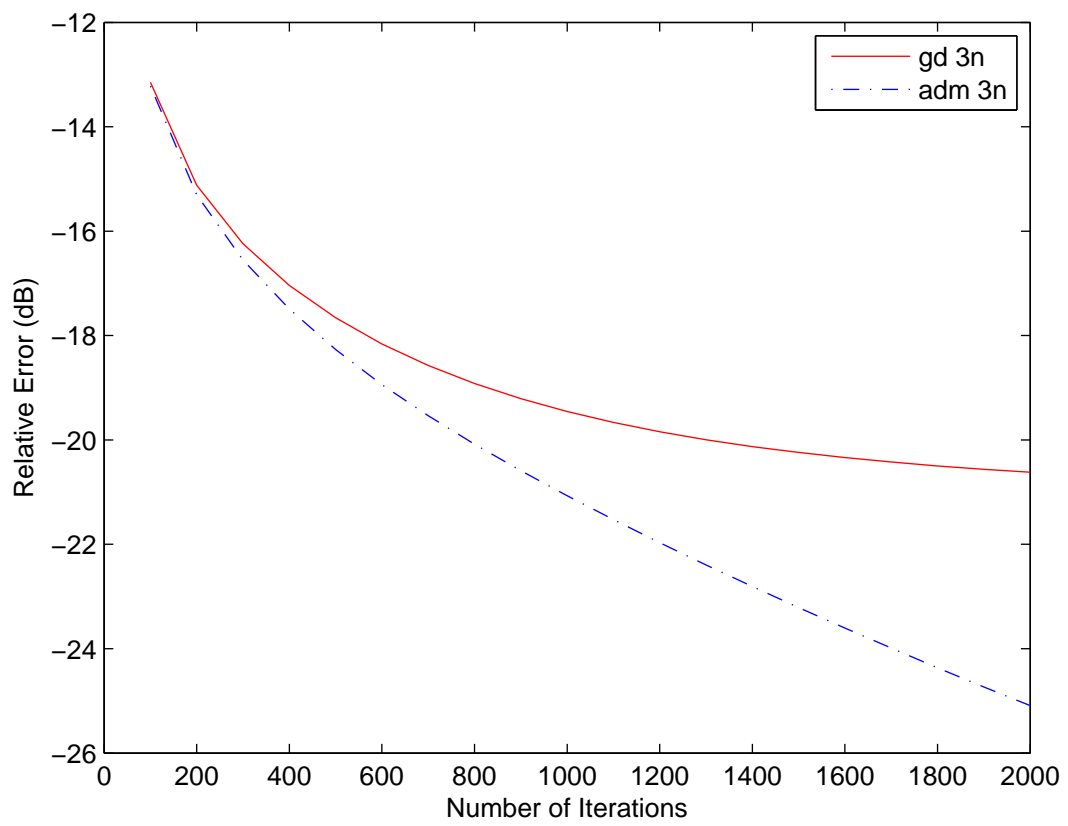


Figure 5.10: Comparison between gradient descent method for 3 η 's.

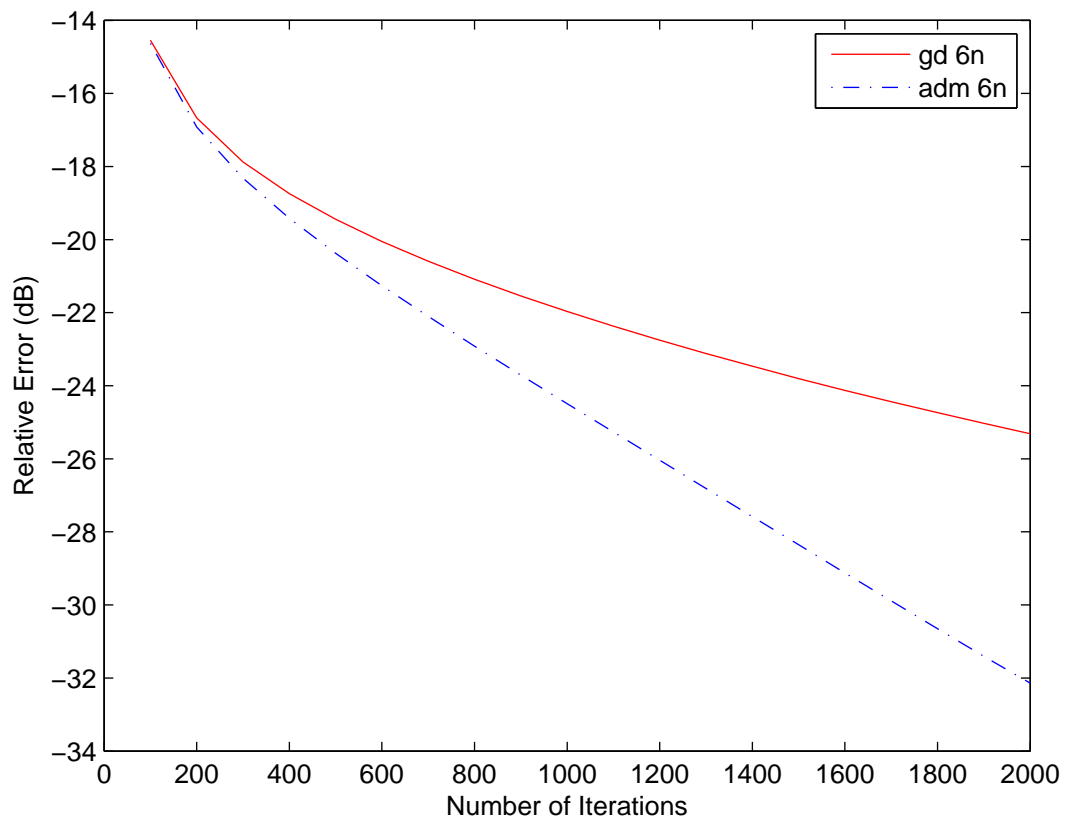


Figure 5.11: Comparison between gradient descent method for 6 η 's.

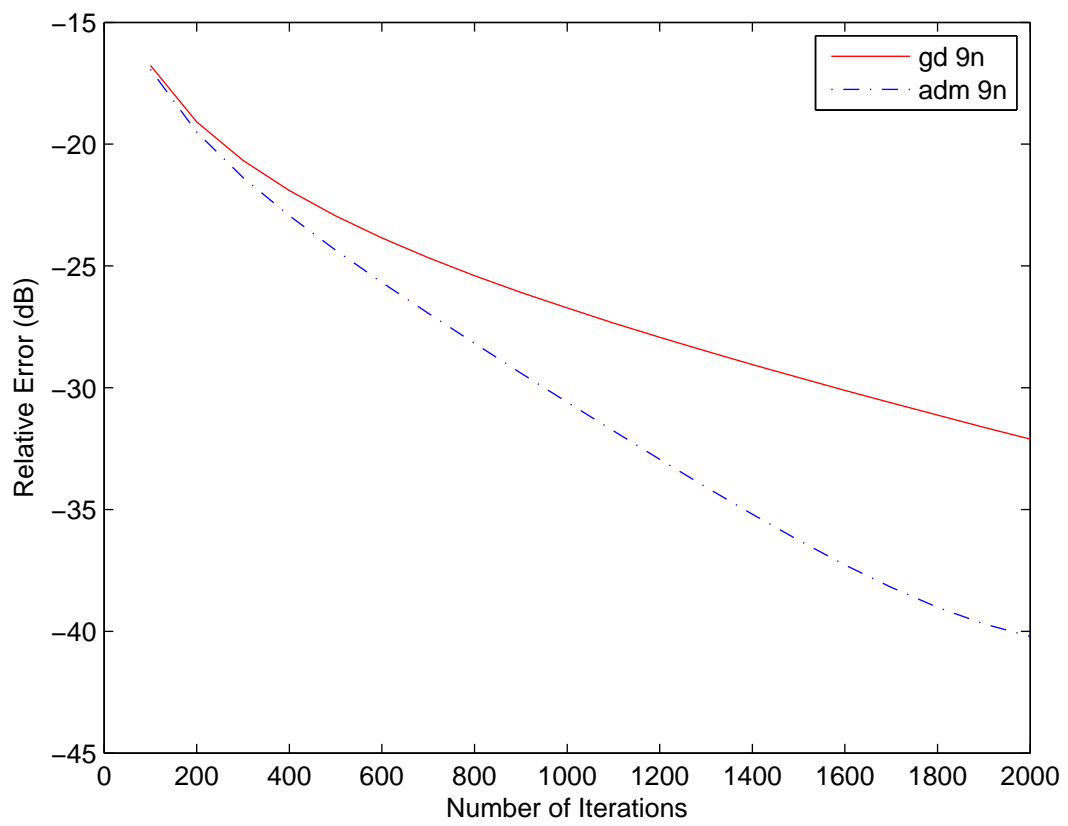


Figure 5.12: Comparison between gradient descent method for 9 η 's.

5.3 Summary

From these results, it shows both more TTRT data and TV regularization improve the reconstruction result. More TTRT data help the iteration converges more rapidly. On the other hand, in the results reconstructed by gradient descent method, there are artifacts of high frequency fringes, and TV regularization reduces this effect.



Chapter 6

Conclusion and Future Works

Conclusion. In this paper, we adopt the truncated transverse ray transform model to reconstruct the trace-free part of the dielectric tensor of a photoelastic material. The least-square model for fidelity functional and TV-regularization are introduced for reconstruction. The augmented Lagrangian method is adopted for solving the corresponding minimization problem. The complete data is a truncated transverse ray transform on TS^2 , which is overdetermined. A smaller data set is a subset L of TS^2 , where $L = \bigcup_j^N L_{\eta_j}$, and $L_{\eta} = \{(\xi, x) \in TS^2 \mid (\xi, \eta) = 0\}$. Our numerical tests demonstrates the following things. First, the augmented Lagrangian method converges faster than the gradient method. Second, within the same method, the converge speed is faster for larger N . It is suggested efficiency gains significantly we should choose $N = 6$ or $N = 9$. Third, the least-square fit of the TTRT model with TV regularization give good image quality for piecewise smooth dielectric tensor.

Discussion and Future works.

1. It is interesting to understand the variation of singular values of the resulting measuring matrix with different numbers and choices of η_j . The goal is to find proper η_j 's for a stable reconstruction.
2. It is not known how the proposed method behaves as the collected data is noisy.
3. When the data is far from complete, can the compressed sensing technique be useful?

All these questions remain further study.



Bibliography

- [1] H. ABEN AND C. GUILLEMET, *Photoelasticity of Glass*, Springer-Verlag Berlin Heidelberg, 1993.
- [2] M. BAAKE AND U. SCHLAGEL, *The peano-baker series*. 2010.
- [3] Y. A. KRAVTSOV, O. N. NAIDA, AND A. A. FUKI, *Waves in weakly anisotropic 3d inhomogeneous media: quasi-isotropic approximation of geometrical optics*, *Physics–Uspekhi*, 39 (1996), pp. 129–154.
- [4] W. LIONHEART AND V. SHARAFUTDINOV, *Reconstruction algorithm for the linearized polarization tomography problem with incomplete data*, *Imaging Microstructures: Mathematical and Computational Challenges*, 494 (2009), pp. 131–159.
- [5] R. NOVIKOV AND V. SHARAFUTDINOV, *On the problem of polarization tomography: I*, *Inverse Problems*, 23 (2007), pp. 1229–1257.
- [6] V. SHARAFUTDINOV, *Integral Geometry of Tensor Fields*, Walter de Gruyter, 1994.
- [7] —, *Slice-by-slice reconstruction algorithm for vector tomography with incomplete data*, *Inverse Problems*, 23 (2007), p. 2603–2627.
- [8] —, *On the problem of polarization tomography: Ii*, *Inverse Problems*, 24 (2008), p. 035010.
- [9] X.-C. TAI AND C. WU, *Augmented lagrangian method, dual methods and split bregman iteration for rof model*, in *Scale Space and Variational Methods in Computer Vision*, X.-C. Tai, K. Mørken, M. Lysaker, and K.-A. Lie, eds., vol. 5567 of

Lecture Notes in Computer Science, Springer Berlin / Heidelberg, 2009, pp. 502–513.

- [10] J. YANG, Y. ZHANG, AND W. YING, *A fast alternating direction method for tvl1-l2 signal reconstruction from partial fourier data*, IEEE Journal of Selected Topics in Signal Processing, 4 (2010), pp. 288–297.

